

UC Santa Barbara

UC Santa Barbara Previously Published Works

Title

Titanite petrochronology of the Pamir gneiss domes: Implications for middle to deep crust exhumation and titanite closure to Pb and Zr diffusion

Permalink

<https://escholarship.org/uc/item/9q96t2rn>

Journal

Tectonics, 34(4)

ISSN

0278-7407

Authors

Stearns, MA
Hacker, BR
Ratschbacher, L
[et al.](#)

Publication Date

2015-04-01

DOI

10.1002/2014TC003774

Peer reviewed

RESEARCH ARTICLE

10.1002/2014TC003774

Key Points:

- Titanite ages record different durations of gneiss dome exhumation from 20 to 8 Ma
- Independent exhumation was driven by two tectonic events rather than GPE alone
- Titanite retained Pb and Zr > 650 C for ~25 Myr

Supporting Information:

- Supporting Information
- Table S1
- Table S2
- Table S3

Correspondence to:

M. A. Stearns,
mstearns@umail.ucsb.edu

Citation:

Stearns, M. A., B. R. Hacker, L. Ratschbacher, D. Rutte, and A. R. C. Kylander-Clark (2015), Titanite petrochronology of the Pamir gneiss domes: Implications for middle to deep crust exhumation and titanite closure to Pb and Zr diffusion, *Tectonics*, 34, 784–802, doi:10.1002/2014TC003774.

Received 10 NOV 2014

Accepted 25 MAR 2015

Accepted article online 30 MAR 2015

Published online 28 APR 2015

Titanite petrochronology of the Pamir gneiss domes: Implications for middle to deep crust exhumation and titanite closure to Pb and Zr diffusion

M. A. Stearns¹, B. R. Hacker¹, L. Ratschbacher², D. Rutte², and A. R. C. Kylander-Clark¹

¹Department of Earth Science, University of California, Santa Barbara, USA, ²Geologie, TU Bergakademie Freiberg, Freiberg, Germany

Abstract The Pamir Plateau, a result of the India-Asia collision, contains extensive exposures of Cenozoic middle to lower crust in domes exhumed by north-south crustal extension. Titanite grains from 60 igneous and metamorphic rocks were investigated with U-Pb + trace element petrochronology (including Zr thermometry) to constrain the timing and temperatures of crustal thickening and exhumation. Titanite from the Pamir domes records thickening from ~44 to 25 Ma. Retrograde titanite from the Yazgulem, Sarez, and Muskol-Shatput domes records a transition from thickening to exhumation at ~20–16 Ma, whereas titanite from the Shakhadara dome records prolonged exhumation from ~20 to 8 Ma. The synchronous onset of exhumation may have been initiated by breakoff of the Indian slab and possible convective removal of the Asian lower crust and/or mantle lithosphere. The prolonged exhumation of the Shakhadara and Muztaghata-Kongur Shan domes may have been driven by continued rollback of the Asian lithosphere concurrent with shortening and northwestward translation of the Pamir Plateau.

1. Introduction

The India-Asia collision zone—especially the Himalaya and the Tibetan Plateau (Figure 1a)—has profoundly shaped our understanding of continent-continent collisions and orogenic plateaux evolution. Despite this prominence, processes at middeep crustal levels are not well understood because the Cenozoic middle to lower crust is exposed only locally within the Tibetan Plateau. In contrast, the Pamir Plateau (Figure 1a) contains large exposures of middle to lower crustal rocks in a series of domes [Robinson *et al.*, 2004; Schwab *et al.*, 2004; Schmidt *et al.*, 2011; Stübner *et al.*, 2013a]. These domes—and the well-studied tectonic framework of the India-Asia collision—provide the opportunity to directly investigate middle to lower crustal processes during the transition from thickening to collapse in an orogenic plateau. This paper presents a U-Pb titanite record of middle to lower crustal burial and exhumation and the implications for Pb and Zr retention in titanite and proposes some possible driving mechanisms for gneiss dome genesis in the Pamir Plateau.

Orogenic plateaux may collapse when gravitational potential energy (GPE) overcomes compressive boundary forces [Molnar and Lyon-Caen, 1988; Rey *et al.*, 2001; Selverstone, 2004]. Changes in GPE come from changes in material thickness, elevation, and density. Significant changes in the boundary forces during continent-continent collisions may arise from processes such as slab breakoff, slab rollback, and foundering of convective instabilities. The rate of orogen collapse is determined by the imbalance of forces and material properties, which are dictated primarily by changes in temperature, composition, and phase (e.g., melting). In this paper, we assess whether collapse of the Pamir Plateau can be tied to changes in regional plate motions by measuring the U-Pb ages and trace element contents (primarily Zr) of titanite in the Pamir middle to lower crust.

Titanite has some important advantages for dating crustal rocks: it occurs in a wide variety of rock types; it may grow or recrystallize during amphibolite-facies prograde and retrograde reactions [Rubatto and Hermann, 2001]; it incorporates abundant uranium in quartzofeldspathic rocks [Frost *et al.*, 2001; Spencer *et al.*, 2013]; it partitions Zr as a function of pressure and temperature, enabling use as a thermobarometer [Hayden *et al.*, 2008]; and it participates in a wide variety of other metamorphic reactions [Frost *et al.*, 2001]. These qualities make it an ideal phase for investigating the history of the Pamir domes (Figure 1b), which are dominated by amphibolite-facies quartzofeldspathic rocks [Vlasov *et al.*, 1991; Robinson *et al.*, 2004; Schwab *et al.*, 2004]. Recent analytical developments make coupled U-Pb + trace element petrochronology [Kylander-Clark *et al.*, 2013]

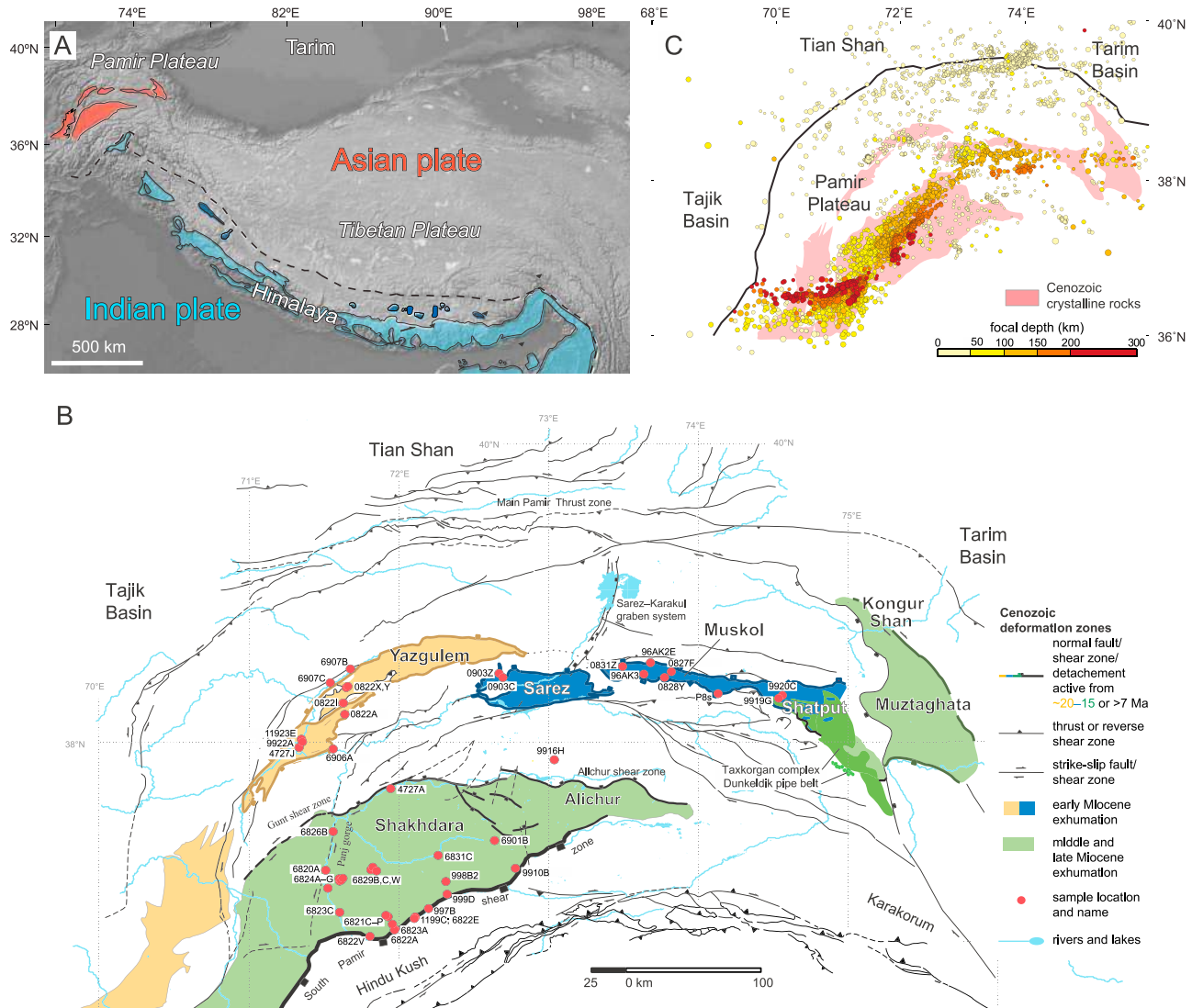


Figure 1. (a) The Pamir Plateau is the western extension of the India-Asia collision zone. Extensive exposures of the Cenozoic Asian middle to lower crust (shown in red) only occur in the Pamir Plateau. Similar exposures of the Indian middle to lower crust (shown in blue) are concentrated in the Himalaya. (b) The Yazgulem, Sarez, and Muskol-Shatput domes of the Central Pamir, and the Shakh dara-Alichur dome in the South Pamir extend across most of the Pamir Plateau. Sample locations (red circles) were chosen to give the widest coverage possible. (c) Earthquake locations show the position of subducting Asian lithosphere (data from Sippl *et al.* [2013a]).

a powerful tool for fingerprinting the timing and temperature of petrogenetic processes and more accurately understanding tectonic processes.

We show that titanites record a prograde/burial through retrograde/exhumation history in the Pamir gneiss domes from ~ 44 to ~ 8 Ma. Burial transitioned to exhumation at ~ 20 Ma, perhaps because of breakoff of the Indian slab. We relate the high-temperature, exhumation-related retrograde metamorphism responsible for titanite (re)crystallization that persisted across the Shakh dara dome until ~ 7 Ma to northward rollback of Asian lithosphere beneath the Pamir (Figure 1c) or foundering of convective instabilities, and collapse of the margin of the Pamir Plateau into the adjacent Tajik Basin [Stübner *et al.*, 2013a]. Temperatures of nearly 700°C sustained for at least ~ 10 Myr were insufficient to reset Pb and Zr in titanite, indicating higher closure temperatures than the commonly assumed range of $600\text{--}700^\circ\text{C}$.

2. Geologic Setting

The Pamir Plateau, the northwestern extension of the Tibetan Plateau, has a crustal thickness of $\sim 60\text{--}75$ km and an average elevation of ~ 4 km [Mechie *et al.*, 2012; Schneider *et al.*, 2013]. Much of this thickening and uplift

occurred during the India-Asia collision [Burtman and Molnar, 1993; Bershaw et al., 2012], driven by 600–900 km of Cenozoic shortening within the Pamir [Schmidt et al., 2011]. The northern margin of the Plateau, the Main Pamir Thrust zone (Figure 1b), accommodates 10–15 mm/yr present-day ~N-S shortening [Reigber et al., 2001; Mohadjer et al., 2010; Zubovich et al., 2010; Ischuk et al., 2013]. This shortening is coupled to northwestward rollback of ~90–250 km of Asian lithosphere (the Pamir slab)—as inferred from receiver functions, local earthquake tomography, and intermediate-depth seismicity [Schneider et al., 2013; Sippl et al., 2013a, 2013b]. Presently, the downdip end of this subducting Asian lithosphere is situated roughly beneath the southwestern Pamir (Figure 1c). The southern limit of the Plateau, the Chitral Himalaya and Hindu Kush, accommodates a similar rate of shortening, 10–15 mm/yr [Mohadjer et al., 2010; Ischuk et al., 2013]. The southern part of the Plateau is underlain to an unknown extent by underthrusting Indian lithosphere [Li et al., 2008; Sippl et al., 2013b]. The interior of the Pamir is experiencing 5–10 mm/yr of ~E-W extension that is matched by shortening in the Tajik Basin west of the Pamir; there is relatively little present-day motion between the Pamir and the Tarim Basin to the east [Mohadjer et al., 2010; Zubovich et al., 2010; Ischuk et al., 2013]. Thus, material—driven by the NNE motion of the Indian Plate—is flowing into the Pamir Plateau from the south and overriding the Tajik Basin. The consequences of this flowing material are the northwestward rollback of the Pamir slab in the deep crust and mantle and the velocity field of the uppermost crust recorded by GPS.

Two belts of large crystalline domes within the Pamir expose amphibolite- to granulite-facies rocks exhumed from depths of 30–40 km [Robinson et al., 2007; Schmidt et al., 2011; Stübner et al., 2013a, 2013b]. U/Th-Pb monazite and Lu-Hf garnet ages from these rocks suggest that crustal thickening began ≥ 37 Ma and that a switch from burial to exhumation occurred at ~20 Ma [Schmidt et al., 2011; Stearns et al., 2013; Smit et al., 2014]. Exhumation by ~N-S crustal extension is directly dated within the largest of the crystalline domes, the composite Shakh dara-Alichur dome (Figure 1b), at ~20–2 Ma [Stübner et al., 2013b]. Additionally, ~E-W extension within the Pamir, which began ~7–8 Ma [Robinson et al., 2004], stands in contrast to the 600–900 km of long-term Cenozoic shortening within the Pamir and indicates a distinct shift in kinematics that may—as intimated above—be linked to changes in GPE, boundary forces, or rheology. Peaking in the mid-Miocene and Pliocene, a thick wedge of coarse clastic sediment was shed into the Tajik Basin, suggesting loading of that basin by (north)westward growth of the Pamir [Schwab et al., 1980; Nikolaev, 2002]. In the following, we group the domes by their shared Cenozoic exhumation histories.

2.1. Yazgulem, Sarez, and Muskol-Shatput Domes

The Yazgulem, Sarez, and Muskol-Shatput domes (Figure 1b) comprise folded and ductilely deformed (D_1 fabric) Paleozoic to Mesozoic marbles and siliciclastic rocks. Mesozoic and Cenozoic gabbroic to granitic intrusions were emplaced before and during regional shortening [Schwab et al., 2004; Stearns et al., 2013]. Prograde upper-amphibolite-facies metamorphism (6–10 kbar and 600–750°C; Schmidt et al., 2011) occurred from ~30 to 15 Ma [Stearns et al., 2013] during the development of the D_1 fabric, which include microscopic-scale foliation and shortening structures. Garnet amphibolites and kyanite + garnet + biotite \pm staurolite metapelites are characterized by initial syndeformation growth of garnet. The metapelites contain synkinematic kyanite (syn- D_1) and local staurolite as well, overprinted by postkinematic kyanite (post- D_1 , preretrograde) and retrograde andalusite and sillimanite. The retrograde mineral assemblage within the amphibolites is characterized by resorbed garnet and pyroxene, ilmenite and rutile breakdown to titanite, chlorite, and local retrograde biotite and amphibole growth.

Discordant Cenozoic aplite and pegmatite dikes and sparse intermediate to felsic plutons crosscut D_1 structures within the domes and increase in abundance toward the dome cores. The dikes are typically nondeformed and contact metamorphosed their host rocks (e.g., static sillimanite overprint of kyanite). The deformation within the domes culminated in ~N-S extension that imprinted a mostly shallowly dipping, typically penetrative D_2 fabric that overprinted D_1 . Mylonitized quartz and feldspar within the D_2 fabric typically transitions from ductile to brittle over tens to hundreds of meters toward the dome-bounding normal-slip shear zones. Forethrust and backthrust reactivated the dome-bounding extensional structures, and open to tight folds (D_3 fabric) affected the earlier fabrics.

2.2. Muztaghata-Kongur Shan and Shakh dara-Alichur Domes

The Cenozoic Muztaghata-Kongur Shan dome exposes mid-Miocene metamorphic rocks exhumed from ~30 km depth by early ~N-S extension across the Shen-ti normal fault followed by ~E-W extension along

the Kongur Shan extensional system [Brunel *et al.*, 1994; Robinson *et al.*, 2004, 2007; Cao *et al.*, 2013; Thiede *et al.*, 2013]. The core of the dome underwent crustal thickening and prograde amphibolite-facies metamorphism from ~33 to 20 Ma and reached peak metamorphic conditions (9–10 kbar, 700–750°C) in the early Miocene. Migmatization occurred at ~14 Ma, followed by exhumation of the Kongur Shan footwall through $^{40}\text{Ar}/^{39}\text{Ar}$ mica, U/Th-He in zircon (ZHe), and apatite fission track closure from ~8 to 1 Ma [Robinson *et al.*, 2007; Thiede *et al.*, 2013].

The Shakh dara-Alichur domes expose the largest area of Cenozoic middle to lower crustal rock in the Pamir. The domes were inundated by arc magmatism during the Cretaceous and are dominated by orthogneiss and intrusive rocks [Schwab *et al.*, 2004; Stübner *et al.*, 2013a, 2013b]. The Cretaceous magmatic arc rocks now exposed in Shakh dara dome experienced contraction (D_1) prior to and synchronous with upper-amphibolite-granulite-facies metamorphism (5.5–15 kbar and 600–800°C; Schmidt *et al.*, 2011) that culminated in extensive migmatization. The Shakh dara dome gneisses were exhumed by top SSE shear along the ~30° south-southeast dipping South Pamir shear zone (SPSZ), which bounds the dome in the south. Flow within the SPSZ occurred continuously from melt-present to brittle conditions. The Panj gorge exposes the footwall of the SPSZ in the core of the dome (Figure 1b). The northern dome boundary comprises a mostly low-grade deformation belt, the Gunt shear/fault zone, where early top to approximately north transtensional shear fabrics were folded into a subvertical zone and overprinted by dextral shear. The smaller Alichur dome is bounded in the north by the Alichur shear zone, which exhumed rocks from 10 to 20 km depth. The Shakh dara and Alichur domes are separated by a low-strain, fault-segmented horst (Figure 1b). Cooling of the Shakh dara dome through $^{40}\text{Ar}/^{39}\text{Ar}$ mica closure began at ~20 Ma in the north (near the Gunt shear zone) and progressed southward from ~16 to 6 Ma along the dome-spanning SPSZ. NNE-SSW extension lasted until ~4–2 Ma [Stübner *et al.*, 2013b], when it was replaced by active ~N-S shortening and ~E-W extension, imprinting the Sarez-Karakul graben system and distributed sinistral-transtensional faults across the western Pamir (Figure 1b) [Schurr *et al.*, 2014].

2.3. Taxkorgan Complex and Dunkeldik Pipe Belt

The Taxkorgan intrusive complex (Figure 1b), in and adjacent to the southwestern margin of the Shatput dome, contains alkalic and granitic intrusive rocks ranging from ~13 to 8 Ma [Xu *et al.*, 1996; Luo *et al.*, 2003; Lin *et al.*, 2006; Ke *et al.*, 2006, 2008; Robinson *et al.*, 2007; Jiang *et al.*, 2012].

The ultrapotassic Dunkeldik magmatic field (Figure 1b) [Dmitriev, 1976] is located in the Central Pamir, southwest of the Shatput dome. The rocks range from dikes and pipes to subvolcanic bodies and volcanic rocks. These rocks erupted at ~11 Ma [Hacker *et al.*, 2005] and contain crustal xenoliths comprising Pamir crustal rocks that experienced peak metamorphic pressures equivalent to 90–100 km depth [Hacker *et al.*, 2005; Gordon *et al.*, 2012].

3. Petrochronology Method

By dating titanite associated with prograde and retrograde metamorphic reactions, and with the D_1 and D_2 deformation fabrics, the P - T - D - t paths can be extracted for each dome. The timing of prograde metamorphism was determined by dating titanites (i) within locally generated leucosomes associated with migmatization, (ii) involved in prograde reactions such as the growth of ilmenite from the breakdown of titanite, and (iii) included within prograde minerals such as garnet (Figure 2a). The timing of retrograde metamorphism, interpreted as coeval with exhumation, was determined by dating titanites that (i) formed during retrogression of rutile and ilmenite (Figures 2b–2d) and (ii) were dynamically recrystallized in the D_2 extensional fabric (Figure 2e). Igneous titanite from nondeformed aplite dikes was dated to place upper and lower bounds on the timing of extension (Figure 2f). We measured U-Pb dates by LA-MC-ICP-MS (laser ablation multicollector inductively coupled plasma mass spectrometry), U-Pb dates + trace elements by LASS (laser ablation-split stream ICP-MS), and additional Zr contents by electron probe microanalysis.

3.1. LA-MC-ICP-MS and LASS

Sixty samples were analyzed from the four gneiss domes (Figure 1b and supporting information Table S1). The majority of samples were dated using LA-MC-ICP-MS; a subset of six samples was dated using LASS [Kylander-Clark *et al.*, 2013]. Typical excimer laser (193 nm wavelength) settings were 30–100% of 3 mJ, 4 Hz repetition rate, and a 25–40 μm diameter laser spot. The resulting laser ablation pits are ~10 μm deep.

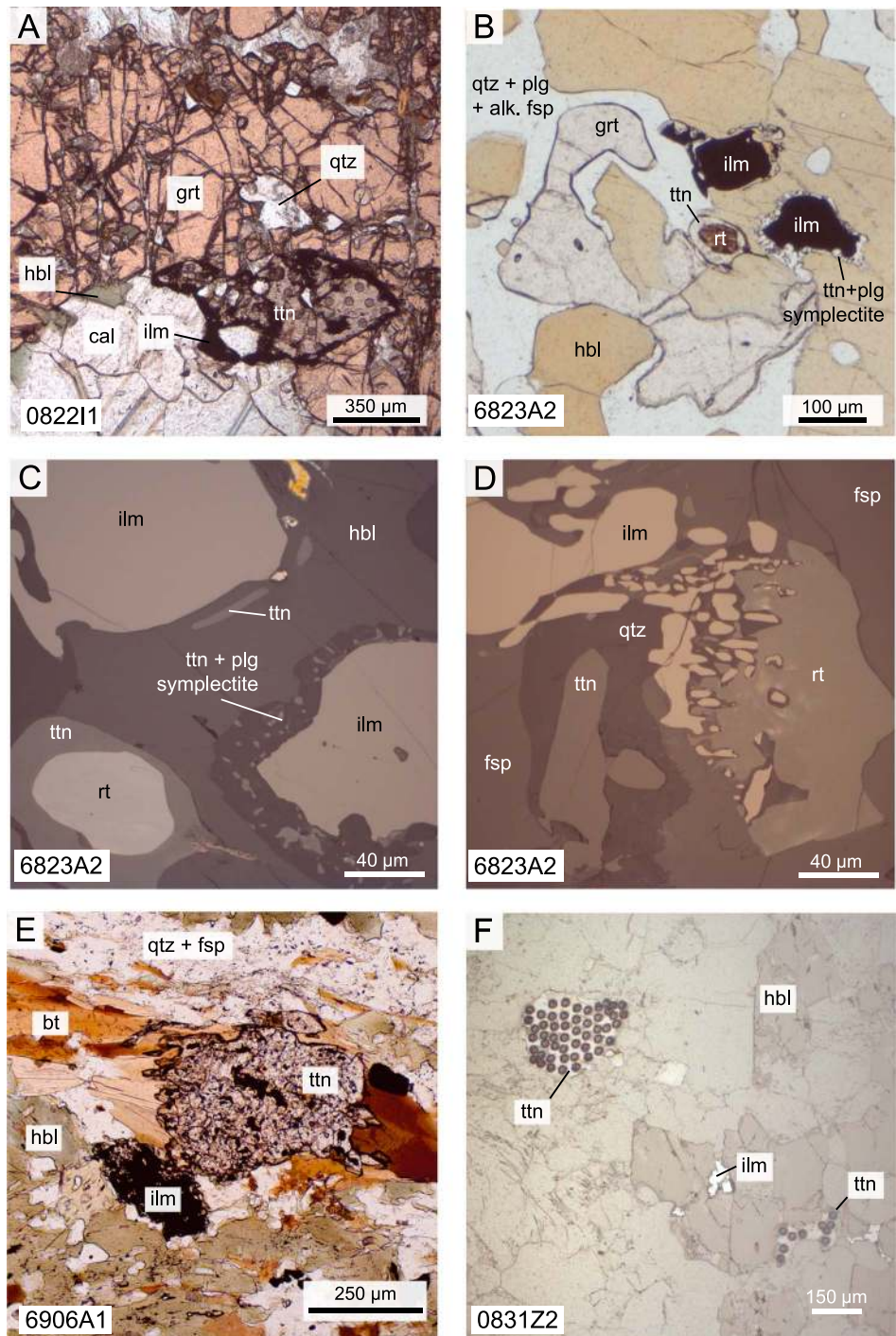


Figure 2. Titanite textures in thin section: (a) 32.4 ± 0.8 Ma titanite breaking down to ilmenite and titanite partly included within garnet are interpreted to date prograde metamorphism in the Yazgulem dome. (b–d) Retrogressed amphibolite after garnet granulite that is interpreted to have melted based on the reaction rims and acute grain boundaries. In Figure 2b, 8.9 ± 0.4 Ma single-age titanite forms retrograde rims on rutile and ilmenite. In Figure 2c, 8.9 ± 0.4 Ma titanite formed by breakdown of rutile and ilmenite. In Figure 2d, complex reaction textures between coexisting rutile, ilmenite, and titanite illustrate the difficulty of determining a single titanite-forming reaction. These titanites are interpreted to record decompression melting during retrograde metamorphism of the southern Shakh dara dome. (e) Dynamically recrystallized titanite porphyroclast formed by the breakdown of ilmenite. The 19.5 ± 0.4 Ma age is interpreted to record onset of exhumation in the Yazgulem dome and the timing of high-T extensional deformation. (f) Titanites between ~ 100 and $400 \mu\text{m}$ with many dating spots yielded a single age of $\sim 17.3 \pm 0.5$ Ma. These titanites within a group of float amphibolites from the far western Muskol-Shatput dome formed by breakdown of ilmenite during retrograde metamorphism.

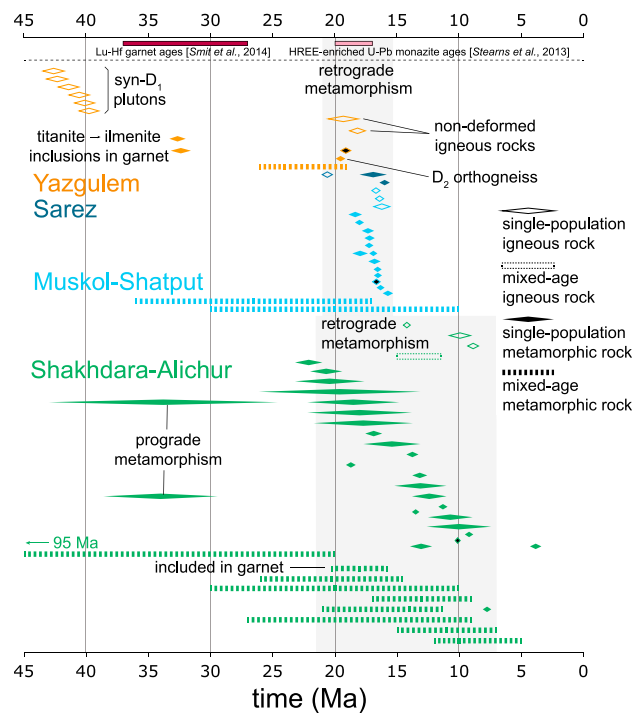


Figure 3. U-Pb titanite dates from the Pamir. Synshortening igneous titanite crystallized in the Yazgulem, Sarez, and Muskol-Shatput domes from 43 to 40 Ma. Titanite records prograde metamorphism in these and the Shakh dara dome around 33 Ma. Retrograde titanite (re)crystallized in the Yazgulem, Sarez, and Muskol-Shatput domes during exhumation (grey bands) from 21 to 15 Ma; more-protracted retrogression and exhumation in the Shakh dara dome was recorded by 22–8 Ma titanite. Black-filled ages were previously reported in *Schmidt et al.* [2011].

et al., 2007; *Mazdab*, 2009; *Spencer et al.*, 2013] and NIST 610 glass [*Gao et al.*, 2007] were used as secondary reference materials. Atomic number, absorption, and fluorescence corrections were made assuming an ideal CaTiSiO_5 composition. The Zr detection limit was $\sim 10\text{--}20$ ppm. For further analytical details, see *Spencer et al.* [2013]. Measurement of Zr in titanite is susceptible to secondary fluorescence from zircon: a linear transect away from a $\sim 30\ \mu\text{m}$ diameter zircon showed that secondary fluorescence is significant to a distance of $\sim 40\ \mu\text{m}$ but negligible at more than $\sim 100\ \mu\text{m}$ from the zircon. The area around each titanite Zr measurement was therefore carefully screened for zircon; it is possible, however, that secondary fluorescence affected some of the Zr measurements from out-of-plane zircon.

The Zr-in-titanite thermometer is pressure dependent [*Hayden et al.*, 2008]. Though peak pressures are known for many of the samples by independent determinations [*Schmidt et al.*, 2011], the quoted apparent temperatures were calculated using a pressure of 4 ± 2 kbar because most titanite (re)crystallization occurred during retrograde metamorphism. Two uncertainties were calculated: one that includes analytical error and the reproducibility of the secondary reference materials and a second that includes uncertainty in pressure and the activity of CaZrSiO_5 ; all the thermometry samples contain quartz, zircon, and rutile. Zr thermometry provides not only an apparent temperature but also can be used to distinguish distinct titanite populations and provide further petrogenetic context for interpretation of U-Pb dates.

4. Results

A summary of the titanite U-Pb dates is shown in Figure 3; all of the U-Pb data are provided in supporting information Table S2. We classify our U-Pb dates into three types (Figure 4). (1) *Single ages*, in which all of the U-Pb data define a single isochron with a suitably low mean square weighted deviation (MSWD) to be a single population [*Wendt and Carl*, 1991]; for such samples we report a single age and uncertainty (Figure 4a). (2) *Multiple ages*, in which the U-Pb data define multiple isochrons or age ranges (Figure 4b), at

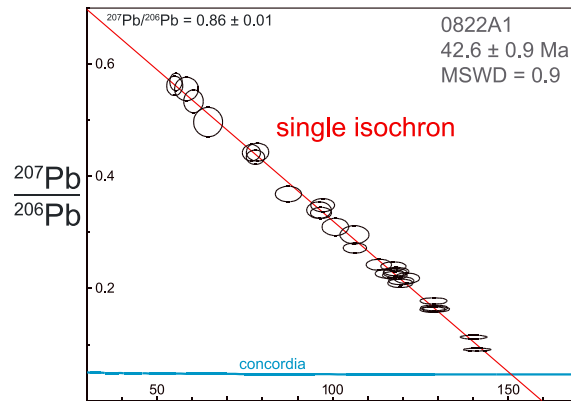
Bear Lake Road titanite [*Aleinikoff et al.*, 2002; *Frost and Fanning*, 2006; *Mazdab*, 2009] was used as the primary reference material, and Y1710C5 [*Spencer et al.*, 2013] was used as the secondary reference material to assess in-run accuracy. The dates reported in this paper have a minimum uncertainty of 2%. For more analytical details, see *Spencer et al.* [2013].

We analyzed the majority of samples in situ in thin section; seven samples were analyzed as titanite separates. Each sample analysis consisted of 20 to 80 single spots from several grains. Each sample also contained analyses of different grain sizes and different portions of large grains to assess variations in age and trace element concentration. Titanite zoning was imaged using backscattered electrons (BSE). Few titanites exhibited internal zoning in BSE images, but where zoning was detected, laser spots were placed entirely within zones to minimize mechanical mixing.

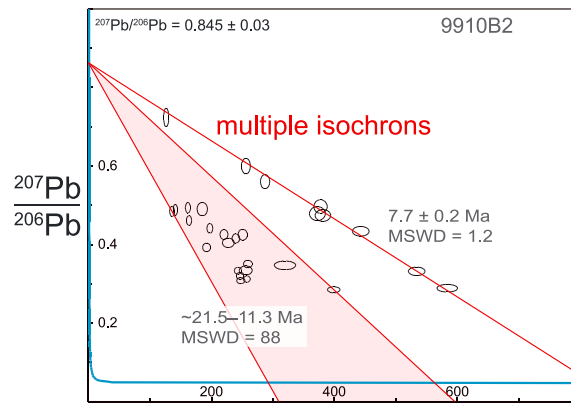
3.2. Electron Probe Microanalysis

Zirconium concentration was measured in titanite with a Cameca SX-100 at 15 kV accelerating voltage and 200 nA beam current. Bear Lake Road titanite [*Aleinikoff*

A. Single age



B. Multiple ages



C. Age range

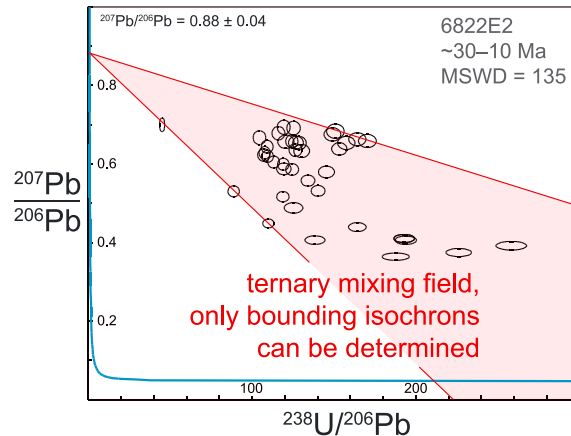


Figure 4. Titanite preserve three different types of U-Pb ages. (a) *Single ages*, with isotopic ratios that form a single population (MSWD = ~1). (b) *Multiple ages*, defined by multiple, single-population arrays. (c) *Age range*, characterized by ternary mixing between a common Pb component and multiple radiogenic Pb components; this can result from continuous (re)crystallization or mechanical mixing during laser sampling.

least one of which has a suitably low MSWD to be a single population. For such samples, multiple ages and uncertainties are reported. (3) *Age ranges*, in which the U-Pb data do not define an isochron or isochrons; for these data we report a range of ^{207}Pb -corrected (sensu *Compston et al.* [1992]) $^{206}\text{Pb}/^{238}\text{U}$ dates (Figure 4c).

Because titanite is often considered to have a whole grain closure temperature of ~600–700°C (see review in *Spencer et al.* [2013]), one might expect that amphibolite-facies titanite would routinely show grain scale gradients in age or that bigger titanite would preserve older ages. Like *Spencer et al.*'s [2013] Norwegian titanites, however, this is not the case for the Pamir titanites—at least at the scale of our laser spots. Instead, we observe four different relationships between age and grain size or position within grains (Figure 5). (1) Pamir titanites with a range of grain sizes that all yield the same age are interpreted to record de novo, or growth of new grains, crystallization or complete recrystallization at temperatures too low for diffusional reequilibration (Figures 2a and 2f). (2) Titanites of a similar size and large enough to accommodate multiple laser spots that all yield the same age are also interpreted to record de novo crystallization or complete recrystallization. (3) Titanites of a uniform grain size that yield an age range may have undergone (i) prolonged de novo crystallization, (ii) incomplete or prolonged recrystallization, or (iii) cooling through a temperature interval conducive to Pb diffusion. (4) Titanites large enough for multiple laser spots that yield multiple ages are interpreted to record multiple crystallizations or partial recrystallization at a scale larger than the 25–40 μm laser spot.

4.1. Yazgulem, Sarez, and Muskol-Shatput Domes Petrochronology

In the carbonate and orthogneiss-dominated *Yazgulem dome* (Figures 3 and 6a), 12 samples were dated. Two garnet amphibolites (082211 and 082212) yielded single ages of ~33 Ma from titanite within the matrix and included within garnet (Figure 2d). The amphibolites are likely part of the 500–450 Ma bimodal igneous sequence that forms the core of the dome [*Schwab et al.*, 2004]. Eight samples

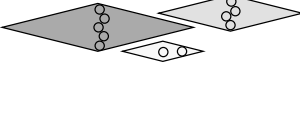
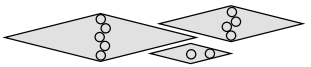
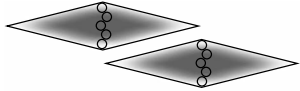

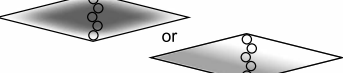
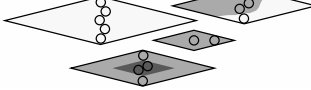
expectations for closure ages	closure-age tests for in situ petrochronology	
A) age covaries with grain size 	observations	interpretations
	1) range of grain size & single age 	i) de novo crystallization ii) complete recrystallization
B) age covaries with spot position 	2) uniform grain size, many spots, & single age 	i) de novo crystallization ii) complete recrystallization
	3) uniform grain size, many spots & age range 	i) prolonged (re)crystallization ii) incomplete recrystallization iii) volume diffusive loss of Pb
	4) many spots & multiple ages 	i) partial recrystallization ii) multiple crystallization events

Figure 5. Interpretation of ages in high-resolution spot dating. If a sample age results from mineral closure to thermally mediated volume diffusion, the grain age should covary with grain size and spot position from core to rim. These hypothetical relationships can be tested by in situ petrochronology by the placement of laser spots that are much smaller than the grain diameter and by analyzing a range of grain sizes.

from seven granitic intrusions yielded single-age titanite spanning ~43–39.5 Ma (8022A, 0822X, and Y; 6907B and C) to ~20.5–17.5 Ma (4727 J and 9922A). Titanites from two mylonitic (normal-sense D_2 fabric) samples record a single age of 19.5 ± 0.2 (orthogneiss 6906A) and an age range of ~26–19 Ma (paragneiss 11923E). We interpret the Yazgulem titanite dates to record granitoid emplacement from ~43 to 39.5 Ma and amphibolite-facies metamorphism at ~33 Ma. Regional metamorphism was followed by granitoid emplacement from ~20.5 to 17.5 Ma, synchronous with the onset of extensional deformation at ~26–19 Ma.

Two samples from the *Sarez* dome were dated (these samples are included in the section across the central Muskol dome, Figures 3 and 6b, because the overall structure of these domes is similar): a garnet amphibolite hornfels (0903Z) that is cut by 2 km scale intrusions within the core of the dome and by a crosscutting pegmatite dike (0903C). Titanite grains from the amphibolite have a single age of 16.0 ± 0.4 Ma. A 12 mm titanite from the crosscutting dike yielded multiple ages: 20.6 ± 0.4 and 16.9 ± 1.1 Ma. These ages correspond to BSE pale and BSE dark zones and are interpreted as emplacement and recrystallization ages, respectively. The titanite ages are interpreted to record dike emplacement at ~20.6 Ma followed by contact metamorphism of the amphibolite and dike at ~16 Ma.

Fifteen samples from the *Muskol-Shatput* dome were dated (Figures 3 and 6b). Garnet amphibolites (0827F4, P8s, 96AK3A, 0827Z, and 0831Z3, which gave two single ages) that form the wall rock to intrusions and are crosscut by dikes have rutile and ilmenite retrogressed to titanite; several titanite grains dated per sample yield an age range of ~36–17 Ma and single ages from ~18.5 to 15.5 Ma. Calcsilicates, schists, and paragneisses contain single-age titanites (0828Y3, 96AK3F, and 9920C2) from 18.4 to 16.2 Ma and one age range of ~30–10 Ma (9919G). Granitoids and dikes (0827F1 and 9920C1), that crosscut the amphibolites and metasediments, have single-age titanites from 16.8 to 15.5 Ma. We interpret the tightly clustered amphibolite dates to record retrograde metamorphism from ~18.5 to 15.5 Ma, closely followed by dike emplacement at ~16.8–15.5 Ma. Amphibolite ages that predate 18.5–15.5 Ma are interpreted to record inheritance from initial titanite crystallization or protracted (re)crystallization during metamorphism.

Titanites from these domes have either homogeneous Zr contents or Zr-rich cores and Zr-poor rims. The cores range from ~200 to 500 ppm Zr and are interpreted to be inherited. The homogenous titanites and rims have ~75–175 ppm Zr (blue data; Figure 7a) and are interpreted to reflect amphibolite-facies retrogression. Despite these petrogenetic differences, the Zr contents correspond to apparent temperatures that overlap within uncertainty: the weighted mean apparent temperature at 4 ± 2 kbar of all samples is $694 \pm 45^\circ\text{C}$ (Figure 7b;

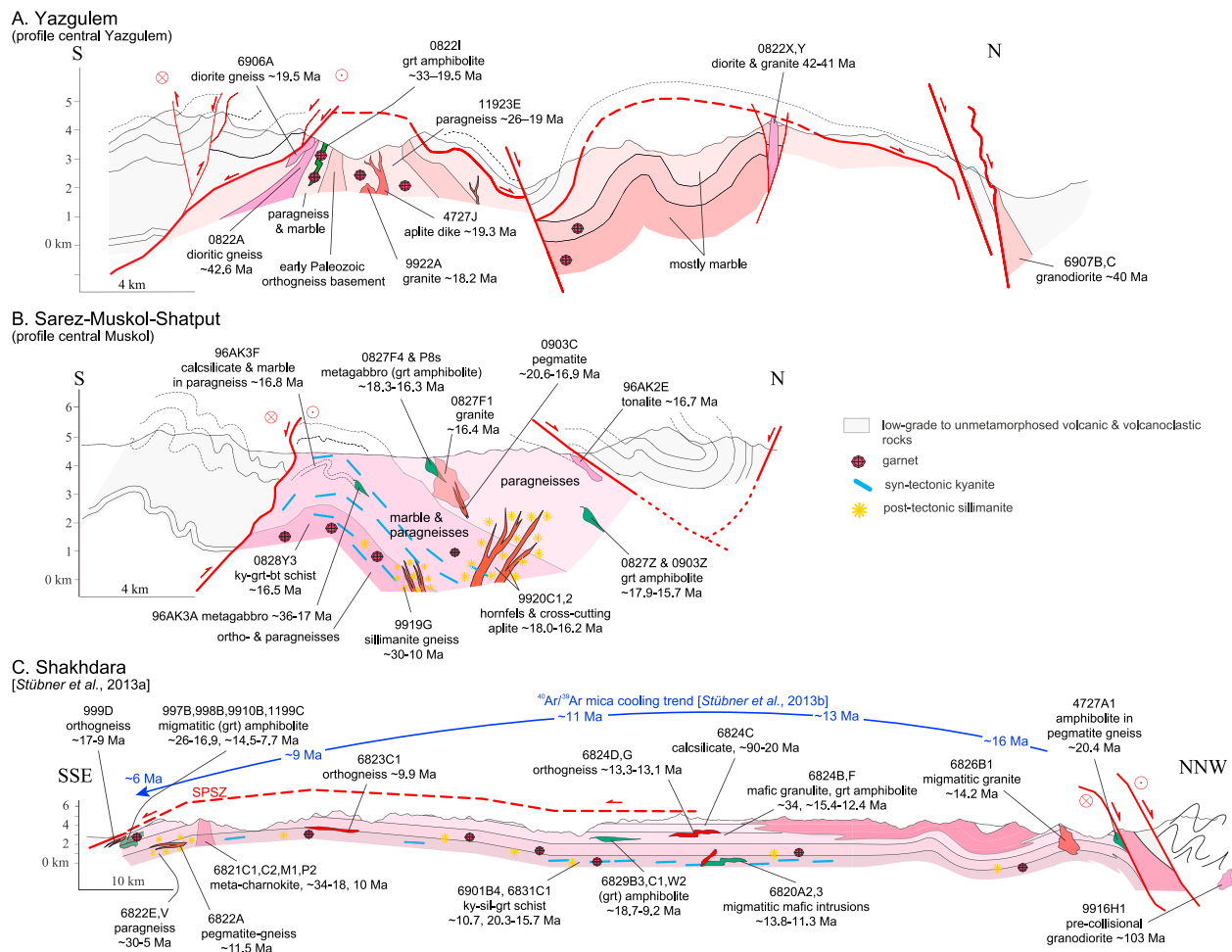


Figure 6. Diagrammatic cross sections placing the analyzed titanites within the structure and lithology of the domes. (a) Yazgulem: ~40 Ma orthogneisses are overprinted by metamorphism and magmatism from ~39 to ~18 Ma. (b) Sarez-Muskol-Shatput: 36–30 Ma metamorphic rocks overprinted by mostly 18–16 Ma metamorphism and magmatism. (c) Shakhudara: 34–30 Ma gneisses overprinted by mostly 18–7 Ma metamorphism and magmatism.

MSWD = 1.1). These apparent temperatures are interpreted as temperatures of titanite (re)crystallization. If a titanite equilibrated during prograde or peak pressures of 8 ± 2 kbar, instead of the 4 ± 2 kbar used in the calculation, the resulting apparent Zr temperature would be 30–40°C higher but still within the quoted uncertainty.

4.2. Shakhudara-Alichur Petrochronology

Thirty-one samples from across the *Shakhudara* dome were analyzed (Figures 3 and 6c), 26 metamorphic rocks and 5 igneous rocks (for some of which multiple dates are reported). The titanites record (1) precollision igneous intrusion (9916H1 and 6823A2), (2) prograde metamorphism from ~34 to 25 Ma (6821C1 and 6824F), (3) nearly continuous retrograde titanite growth (from rutile and ilmenite) from ~25 to 9 Ma, the majority of which are younger than ~22 Ma, and (4) aplite and pegmatite dike emplacement from ~15 to 7 Ma (6820A, 6823A2, 6823C1, 6826B1, and 6822A3). In general, the youngest titanite dates from each sample young toward the South Pamir shear zone (SPSZ; Figure 8a).

The dates come from four different structural domains identified by Stübner *et al.* [2013a] (Figure 1b): the northern bounding Gunt shear zone (GSZ), the southern bounding SPSZ, Panj Gorge dome transect (PGT) that cuts N-S through the western portion of the dome, and central Shakhudara dome. The youngest titanite dates (i.e., a single age or the lower bound of an age range) from the PGT correlate with elevation (Figure 8b). Age-elevation trends (proxy for exhumation rate) do not include all the data but rather were calculated from the “leading edge” of the ages. The youngest SPSZ titanites range from ~17–7 Ma and

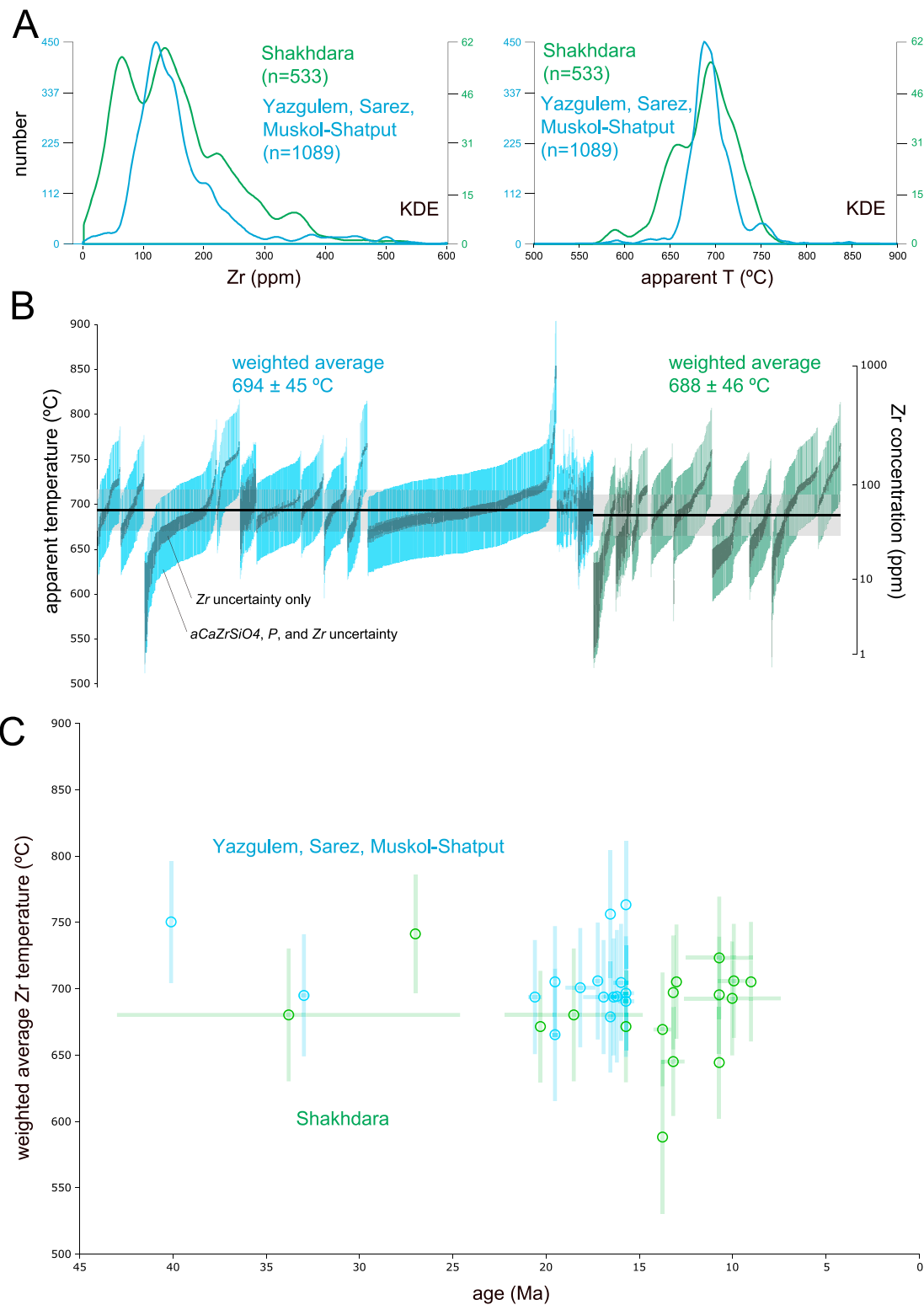


Figure 7. The Zr contents in titanite and Zr-in-titanite temperatures [Hayden *et al.*, 2008] are similar in the Pamir domes and indicate (re)crystallization at amphibolite-facies conditions. (a) Kernel density estimates [Vermeesch, 2012] of all data. (b) Weighted averages of related domes. (c) The temperature-time array, by sample, shows that prolonged amphibolite-facies conditions persisted until ~8 Ma in the Shakh dara dome.

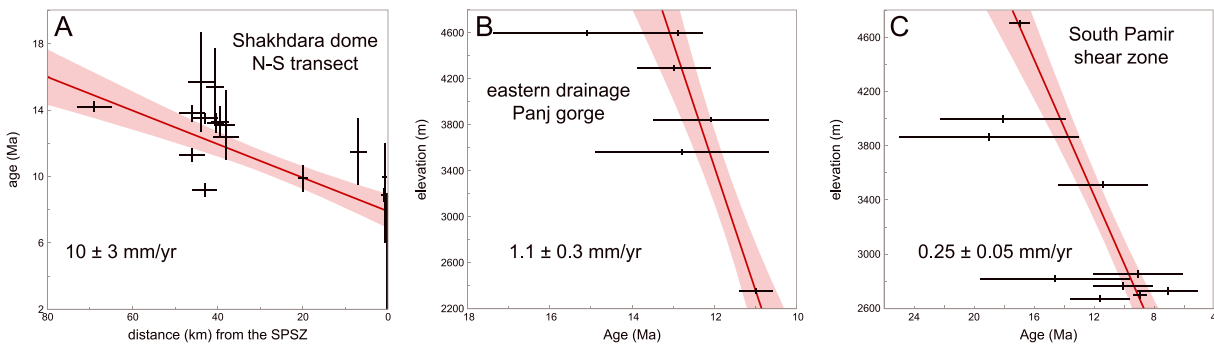


Figure 8. U-Pb age-distance relationship for titanite from transects. (a) NNW-SSE transect across the Shakh dara dome. The 10 ± 3 mm/yr rate is identical to those obtained from $^{40}\text{Ar}/^{39}\text{Ar}$ mica, (U-Th)/He zircon, and apatite fission track dates [Stübner *et al.*, 2013b]. (b, c) Age-elevation transects through the core of the Shakh dara dome (eastern Panj gorge) and near the South Pamir shear zone show long-term cooling similar to that inferred from $^{40}\text{Ar}/^{39}\text{Ar}$ mica ages [Stübner *et al.*, 2013b]. The plotted titanite data are either single ages or the youngest of multiple ages or age ranges from the relevant samples.

span ~ 2250 m. These data overlap the $^{40}\text{Ar}/^{39}\text{Ar}$ dates [Stübner *et al.*, 2013b] and have a similar slope of $\sim 0.25 \pm 0.05$ mm/yr (Figure 8c). Samples from the PGT range from ~ 15 to 8 Ma and span ~ 2250 m ($\sim 1.1 \pm 0.3$ mm/yr). Along the PGT, the titanite dates are older than the $^{40}\text{Ar}/^{39}\text{Ar}$ ages by ~ 3 –4 Myr, and the exhumation rate (1.1 ± 0.3 mm/yr) is faster than the thermochronology-determined exhumation rate of 0.4 ± 0.2 mm/yr. Nearly synchronous retrograde metamorphism in the crustal column could produce a very steep elevation-age profile and thus a rapid apparent exhumation rate. This phenomenon could explain the discrepancy between the (1) the titanite and thermochronology data along the PGT and (2) the difference in apparent exhumation rates along the PGT and the SPSZ.

Although the age-distance and age-depth patterns mirror the thermal structure of the dome [Stübner *et al.*, 2013b], the ages are interpreted to represent (re)crystallization rather than diffusion-controlled mineral closure. The dates represent the timing of retrograde metamorphism related to exhumation that progressed structurally downward and to the south. Titanite records prolonged high-temperature retrograde metamorphism during the tectonic unroofing accomplished by \sim NNE-SSW extension from ~ 15 to 7 Ma. The titanite dates only slightly predate the $^{40}\text{Ar}/^{39}\text{Ar}$ cooling ages but reflect a different process. Coupled with Zr thermometry, the age-elevation trends provide a record of the thermal state of Shakh dara dome during the initiation of exhumation.

Titanites from the Shakh dara dome contain ~ 10 –475 ppm Zr (Figure 7a). Both high-Zr cores/low-Zr rims and low-Zr core/high-Zr rims are present in single-age samples and in samples with an age range. In general, samples with U-Pb ages between ~ 20 and 13 Ma have ~ 60 –150 ppm Zr, whereas samples younger than ~ 12 Ma have ~ 140 –250 ppm Zr. The weighted mean apparent temperature of the ~ 20 –13 Ma population is $671 \pm 43^\circ\text{C}$ (MSWD=0.6), and the < 12 Ma population is $703 \pm 45^\circ\text{C}$ (MSWD=0.3). Again, if peak pressures were instead used for the calculation, the resulting apparent temperature would be ~ 30 – 40°C higher but still within uncertainty. These apparent temperatures record heating and/or decompression after ~ 12 Ma.

Coupled U-Pb and trace element analysis of samples 997B3 and 6822V1 (Figures 9 and 10) shows intrasample chemical variations that correlate with age. Maps of representative clusters of analyses from sample 997B3 (Figure 10a) and sample 6822V1 (Figure 10b) show the spatial relationship of the trace element-age variability. Though sample-wide analyses of sample 997B3 vary continuously from ~ 27 Ma domains with high Zr, Y, and Sr content to ~ 7 Ma domains with low Zr, Y, and Sr (Figure 9), the maps show that the end-member domains with similar age range are often adjacent to one another. As a whole, the variation is continuous but nonlinear. The data were compared to a mixing model (Figure 9) to evaluate whether the trends resulted from mechanical mixing during laser ablation. Though some individual data fall on the mixing curve, the mixing model fails to predict the trace element trajectory for Y and Zr and only fits a portion of the Sr data, suggesting that the elemental variation is the result of continuous reaction or recrystallization and not mechanical mixing. The grain maps of sample 997B3 in Figure 10a are consistent with the concordia plots (Figures 9a and 9b) and show that (1) most older analyses are within the grain cores, but some are near grain rims, and (2) the smallest grains are not the youngest. These observations

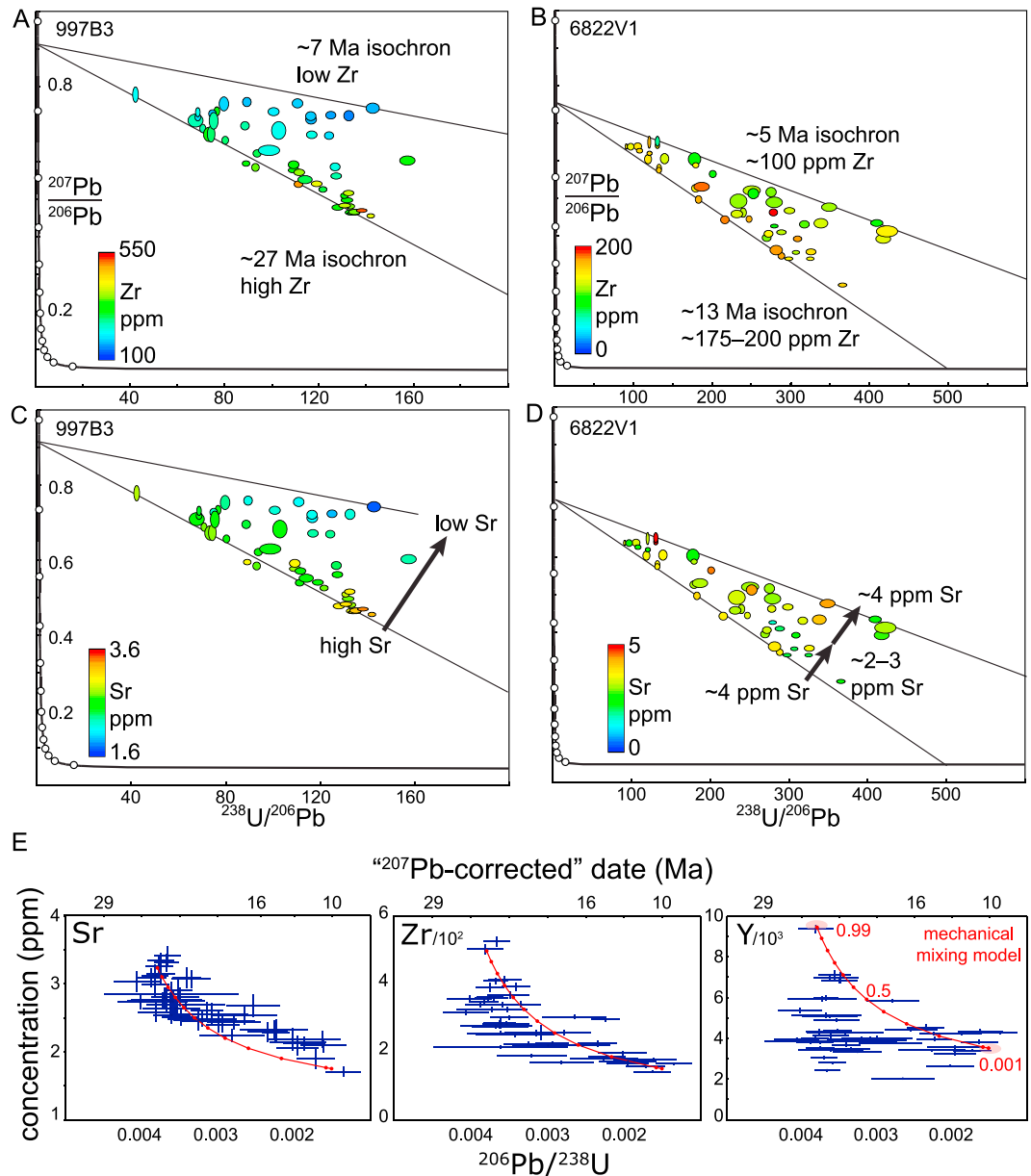
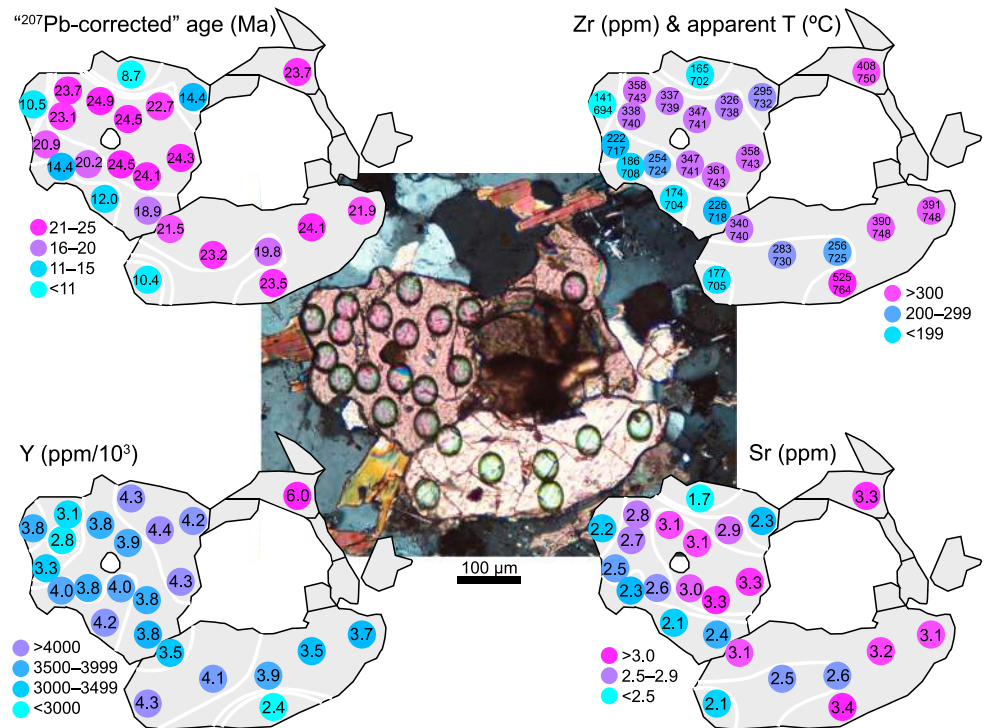


Figure 9. (a–d) Coupled U-Pb and trace element analyses from two samples show variation in Zr and Sr over time. (e) Variation due to mechanical mixing or contamination by inclusions is unlikely: an element-isotopic ratio mixing model shows that only some of the variation (e.g., Sr and Zr) can be attributed to mechanical mixing during laser ablation. The end-members for the mixing model are shown as red ellipses, and the mixing line is labeled with the fractional proportion of the upper end-member (only labeled on the Y plot).

are similar to those outlined in the Figure 5 (#4, center column) and thus are interpreted to record partial or continuous recrystallization at ~ 20 – 6 Ma.

Similarly, sample 6822V1 (Figures 9c, 9d, and 10b) yielded continuous U-Pb dates from ~ 13 to 5 Ma that decrease from ~ 200 to 100 ppm Zr; unlike 997B3, the Sr content decreases from ~ 4 to 2 ppm then increases back to 5 ppm. This pattern in sample 6822V1 could not have been formed by either mechanical mixing or volume diffusion and is interpreted as prolonged titanite (re)crystallization. The grain maps of an aggregate of titanites from sample 6822V1 (Figure 10b) shows similar relationships to 997B3 between grain size, proximity to grain boundary, and resetting, and are also interpreted to record partial or continuous recrystallization from ~ 13 to 5 Ma.

A. 997B3



B. 6822V1

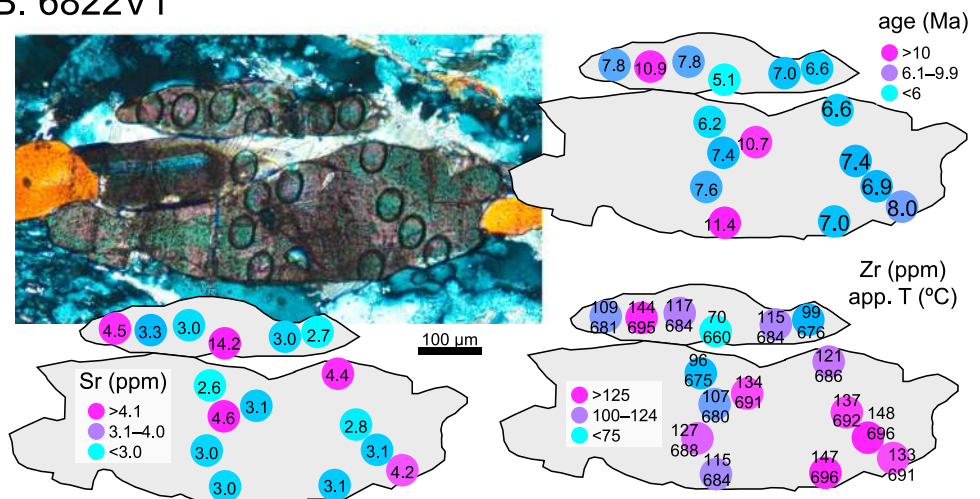


Figure 10. Maps and photomicrographs of a representative cluster of analyses show the spatial relationships (Figure 5) between U-Pb age and trace element compositions. (a) Titanite in sample 997B3 has an older core with more Zr, Y, and Sr. (b) Titanite from sample 6822V1 is more heterogeneous. In both samples the trace element content, age, grain sizes, and spot positions do not follow the predictions outlined in Figure 4 and thus are interpreted as incomplete or prolonged recrystallization.

5. Discussion

5.1. Titanite Closure

Evaluating the role of volume diffusion is an essential aspect of understanding the processes that control the retention and distribution of Pb and Zr in titanite and thus interpreting U-Pb ages and Zr apparent temperatures. Experiments have shown that volume diffusion of Pb [Cherniak, 1993, 2010] is roughly 2 orders of magnitude faster than Zr [Cherniak, 2006; Hayden *et al.*, 2008]. Both experimental and natural

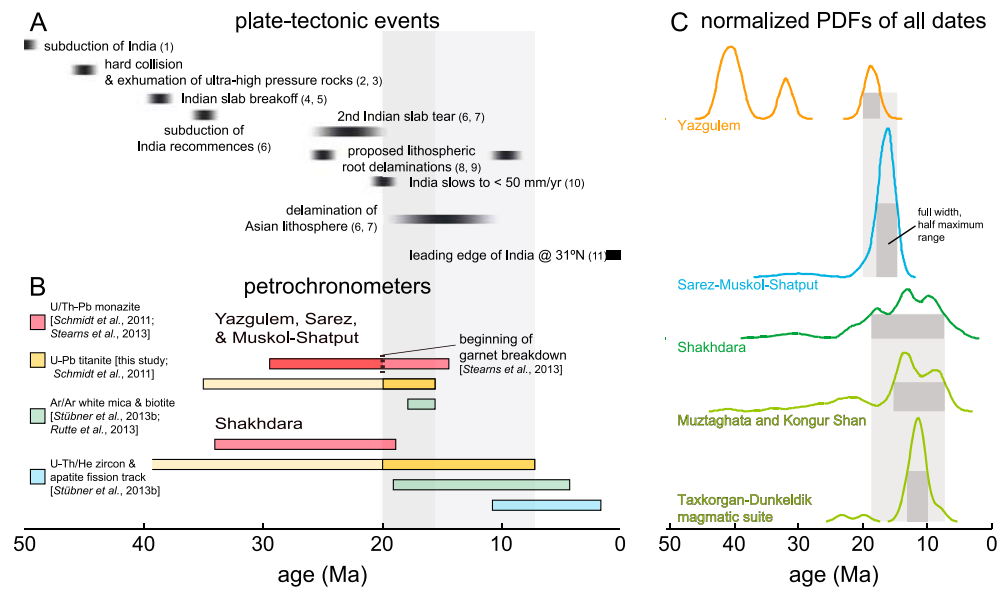


Figure 11. (b) Comparison of the petrochronologic record to (a) independently identified plate tectonic events shows possible driving mechanisms of the metamorphism and exhumation of the Pamir domes. Titanite petrochronology (yellow boxes and shaded bars) from this study places limits on the timing of the transition from thickening to exhumation. (c) Normalized probability density function of all of the published U-Pb and Ar/Ar geochronology from each of the Cenozoic Pamir domes and the Taxkorgan-Dunkeldik volcanic complex illustrates the differences between timing of metamorphism and exhumation of the Yazgulem-Sarez-Muskol-Shatput domes inferred to be driven by breakoff of the Indian slab and the Shakhdara-Muztaghata-Kongur Shan-Taxkorgan events interpreted to be driven by delamination and rollback of the Pamir slab. 1. *van Hinsbergen et al.* [2011], 2. *Lee and Lawver* [1995], 3. *de Sigoyer et al.* [2000], 4. *Kohn and Parkinson* [2002], 5. *Negredo et al.* [2007], 6. *Replumaz et al.* [2010], 7. *DeCelles et al.* [2011], 8. *Chung et al.* [2003], 9. *Chung et al.* [2005], 10. *Copley et al.* [2010], 11. *Nábělek et al.* [2009].

data sets indicate that volume diffusion of Pb and Zr should occur at amphibolite-facies conditions [e.g., *Scott and St-Onge*, 1995; *Corfu*, 1996; *Cherniak*, 2006]. Titanite-bearing metamorphic rocks from the Pamir recorded temperatures of ~700°C for ~10–20 Myr (Figure 7c). Heating of that magnitude and duration should have caused complete diffusive Pb loss from ~1000 μm grains, and larger grains should show Pb zoning at the ~50 μm scale. In contrast to this expectation, titanite from the Pamir retained both Pb and Zr over a prolonged period from >30 Ma to ~7 Ma (e.g., samples 08221, 96AK3, and 6824F).

Nearly all the samples analyzed in this study contain roughly an order of magnitude variation in titanite grain size (Figures 2f, 10a and 10b; ~25–400 μm diameter). Many of the samples with a range of titanite grain size yielded single ages within the spatial resolution of the laser spots (25–40 μm). For the observed range of grain sizes (~50–500 μm), a cooling rate >200°C/Myr is required [*Cherniak*, 1993] to produce a single age by volume diffusion-controlled mineral closure. This hypothetical cooling rate is faster than the ~50–75°C/Myr thermochronology-determined cooling rates from the Pamir [*Stübner et al.*, 2013b]. The patterns of age and chemical variation and the inconsistency between the observed and required cooling rates suggest that U-Pb and Zr were reset by the crystallization of new grains or the recrystallization of existing grains rather than by closure to thermally controlled volume diffusion. These findings highlight the importance of (1) analyzing grains of different sizes, (2) in situ analysis, and the (3) ability to rapidly produce data to populate an isochron by LA(SS)-ICP-MS for distinguishing closure from (re)crystallization. These results support a higher temperature for Pb and Zr closure in titanite [*Schärer et al.*, 1994; *Zhang and Schärer*, 1996; *Gao et al.*, 2012; *Spencer et al.*, 2013] rather than the ~650°C closure temperature predicted by laboratory experiments [*Cherniak*, 1993, 2006].

5.2. Pamir Plate Tectonic Events

Following the initial breakoff of the oceanic part of the Indian slab subducting beneath Asia at ~45 Ma (Figure 11a) [*Kohn and Parkinson*, 2002; *Negredo et al.*, 2007], subduction of a buoyant Indian plate is inferred to have forced the Asian plate into contraction [*Chung et al.*, 2003; *Replumaz et al.*, 2010; *DeCelles et al.*, 2011]. Then, beginning at 32–25 Ma, the lower crust and mantle of the Indian plate is

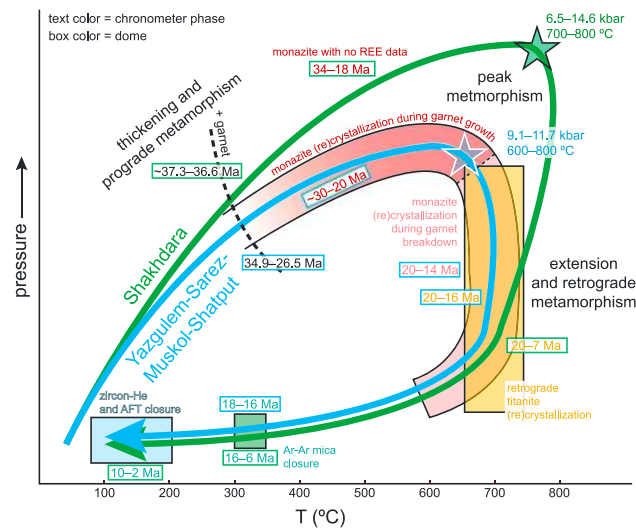


Figure 12. The prolonged exhumation history of Shakhhdara dome relative to Yazgulem-Sarez-Muskol-Shatput domes can be seen as two semi-quantitative P - T - t paths based on the current petrochronology (Lu-Hf garnet, Smit *et al.* [2014]; U-Pb titanite, this study; and monazite, Stearns *et al.* [2013]), thermobarometry (peak P - T determinations shown as stars, Schmidt *et al.* [2011]), and thermochronology (Ar-Ar mica, U-Th/He zircon, and apatite fission track, Stübner *et al.* [2013b]; Rutte *et al.* [2013]) data sets.

and ~35–14 Ma in the Yazgulem, Sarez, and Muskol-Shatput domes (Figures 11b and 12; Schmidt *et al.* [2011]; Stearns *et al.* [2013]; Smit *et al.* [2014]). Depletion/enrichment patterns in heavy rare earth element contents of monazite from the Yazgulem, Sarez, and Muskol-Shatput domes suggests decompression at ~20 Ma. Titanite ages from this study (Figures 3 and 12) associated with cooling/decompression reactions record the beginning of exhumation from ~20 Ma in the Pamir domes and corroborate the interpretation that monazite also record decompression beginning at ~20 Ma. Titanite ages almost entirely overlap with $^{40}\text{Ar}/^{39}\text{Ar}$ mica cooling ages from the Muskol-Shatput dome (Figure 12) [Rutte *et al.*, 2013], suggesting cooling from ~675–750°C (Zr apparent temperatures) through muscovite closure (~350–300°C) in less than 5 Myr. In contrast, few of the titanite and ^{40}Ar - ^{39}Ar ages from the same locality within the Shakhhdara dome overlap; rather, the titanite record prolonged and later peak (re)crystallization at temperatures $\geq 650^\circ\text{C}$ until ~7 Ma (Figures 11b and 12).

The timing of Shakhhdara high-temperature exhumation is similar to the exhumation interval of the Muztaghata (~11–8 Ma) and Kongur Shan (~7 Ma to present) [Robinson *et al.*, 2007] domes and the eruption ages of the Taxkorgan-Dunkeldik subvolcanic and volcanic rocks (Figure 11c). Th-Pb monazite ages and $^{40}\text{Ar}/^{39}\text{Ar}$ mica ages from the footwall of the Kongur Shan extensional system record metamorphism from ~30 to 20 Ma followed by migmatization at ~14 Ma and exhumation from ~11 to 8 Ma. Th-Pb ages from monazites within garnet have a different distribution (~25 Ma mode) than monazites in the rock matrix, which are predominantly younger than ~18 Ma.

The Taxkorgan alkalic complex [Luo *et al.*, 2003; Ke *et al.*, 2008] and Dunkeldik volcanic field [Ducea *et al.*, 2003; Gordon *et al.*, 2012] have eruptive ages between ~13 and 8 Ma with the mode at ~11 Ma (Figure 11c). The common ages of these volcanic complexes and of the rapid exhumation of the Shakhhdara and Muztaghata-Kongur Shan domes suggest that the volcanism and extension were triggered by the same event. Jiang *et al.* [2012] suggested that the Taxkorgan and the Dunkeldik suite magmas both resulted from decompression melting and asthenosphere upwelling following a slab breakoff consistent with the exhumation history of the Pamir crustal xenoliths [Hacker *et al.*, 2005; Gordon *et al.*, 2012].

Combining these inferences with seismic imaging [Mechie *et al.*, 2012; Schneider *et al.*, 2013; Sippl *et al.*, 2013b] leads to the following proposed tectonic evolution. Long-lived northward subduction of Tethyan oceanic lithosphere concluded with the collision and subduction of Indian continental lithosphere. Breakoff of the Tethyan oceanic lithosphere from the Indian continent occurred at ~45 Ma (Figure 13). Subsequent

interpreted to have rolled back southward [Chung *et al.*, 2005; Ding *et al.*, 2005; Kapp *et al.*, 2007]. This is thought to have culminated at ~25–20 Ma in a second breakoff of the underthrust Indian continental slab [Replumaz *et al.*, 2010; DeCelles *et al.*, 2011].

In the Pamir, shortening across the Main Pamir Thrust zone and large-scale dextral strike-slip along its eastern margin commenced at 25–18 Ma [Sobel and Dumitru, 1997; Coutand *et al.*, 2002; Cowgill, 2010] or ~10–6 Ma [Bershaw *et al.*, 2012; Cao *et al.*, 2013]. As rollback of the Asian lithosphere beneath the Pamir is likely partly accommodated by thrusting along the Main Pamir Thrust [Sippl *et al.*, 2013b; Sobel *et al.*, 2013], the rollback probably started not earlier than 25–18 Myr ago.

Lu-Hf garnet and U/Th-Pb monazite ages document prolonged metamorphism from ~37 to 20 Ma in the Shakhhdara

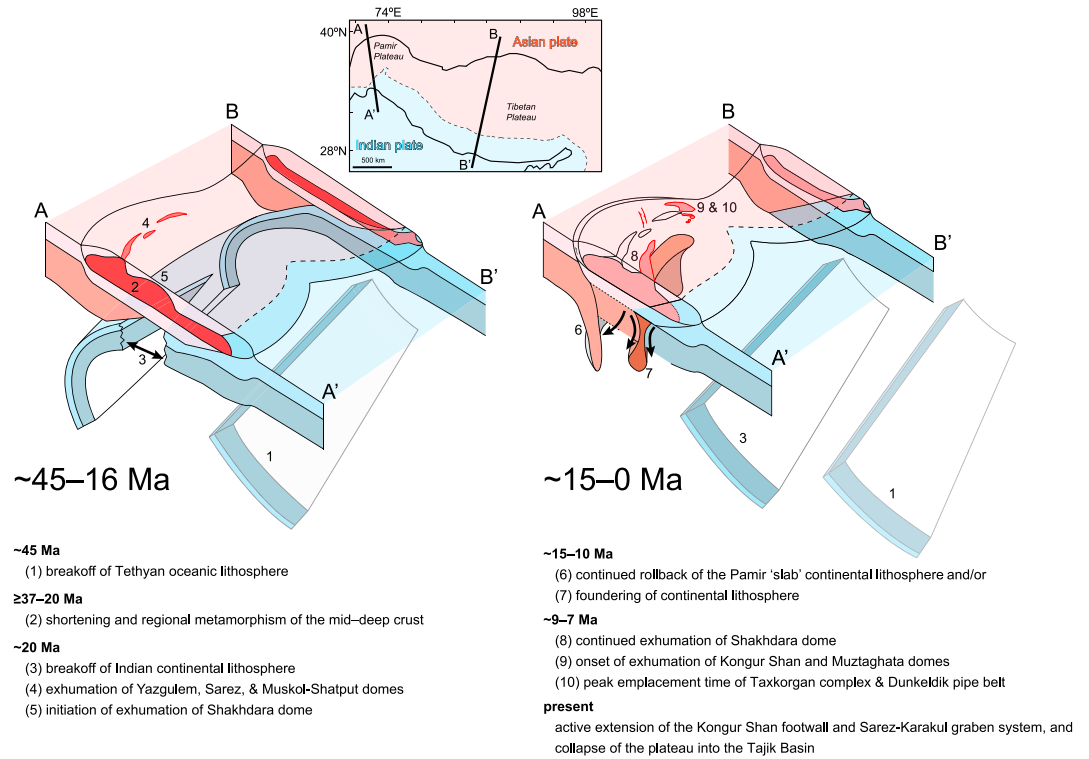


Figure 13. A conceptualized model for the tectonic evolution of the Pamir Plateau and India-Asia collision illustrates the interpreted sequence of events and possible driving mechanisms affecting the orogen. Two generalized cross sections through the Pamir and Tibetan Plateaux bound the block diagram; the area between the two cross sections is transparent in order to visualize subsurface processes.

contraction thickened the Pamir crust from ~37 to 20 Ma. Subduction of Indian continental lithosphere continued until a second rollback and breakoff of the Indian lithosphere beginning ~25–20 Ma (Figure 13). Indian continental lithosphere breakoff, perhaps accompanied by downwelling and convective removal of a dense Asian lithospheric root, resulted in a regional increase of GPE in the Pamir and likely the Hindu Kush and Karakoram further south. Both downwelling and increased GPE may have triggered delamination and rollback of the Asian continental lithosphere (Pamir slab), which drove the Pamir crust from contraction into extension ~20 Ma ago. These changes in boundary forces led to rapid cooling of the middle to deep crust at ~20–16 Ma, best documented in the Yazgulem, Sarez, and Muskol-Shatput domes (Figure 13). Following breakoff and delamination, input of asthenospheric heat into the Pamir lithosphere caused magmatism and prolonged high-grade metamorphism and migmatization best observed in the Shakhdara dome, Taxkorgan complex, Dunkeldik volcanic field, and likely the Hindu Kush and Karakoram [Mahéo *et al.*, 2002]. The resulting thermal weakening of the Pamir crust and further delamination of the Asian lithosphere, which by then was telescoped northward by the indenting Indian lithospheric mantle [Mechie *et al.*, 2012; Sippl *et al.*, 2013b], continued to drive collapse of the Pamir Plateau via crustal extension in the Shakhdara [Stübner *et al.*, 2013a] and the Muztaghata and Kongur Shan domes [Robinson *et al.*, 2004, 2007] and the Sarez-Karakul transtensional graben system [Schurr *et al.*, 2014] into the lowland of the Tajik Basin (Figure 13) [Stübner *et al.*, 2013a]. There has been ~90 km of extension accommodated within the middle to deep crust of the Shakhdara dome, which initiated and was active from ~15 to 7 Ma (this study). Low-temperature thermochronometers from Shakhdara also record extension-related exhumation from ~4 to 2 Ma (Figure 11b) [Stübner *et al.*, 2013b]. At the northeast margin of the plateau, a maximum of 35 km of extension began in the Muztaghata dome from ~11 to 8 Ma and remains active in the Kongur Shan dome (~7 Ma to present) [Robinson *et al.*, 2007]. Active, north-northeast trending, sinistral-transtensional fault systems—dissecting the Pamir’s interior and concentrated along the Sarez-Karakul transtensional graben system and in the western Pamir—trace active collapse [Schurr *et al.*, 2014].

6. Conclusions

Titanite petrochronology, specifically U-Pb ages and Zr-in-titanite thermometry from igneous intrusions and prograde and retrograde metamorphic titanite, documents the transition from crustal thickening to extensional exhumation in the Pamir domes. The early stages of exhumation began synchronously around ~20 Ma but ended asynchronously. The Yazgulem, Sarez, and Muskol-Shatput domes cooled rapidly below ~650°C by ~16 Ma, whereas the Shakh dara dome remained above 650°C until ~10 Ma. The initiation of exhumation across the Pamir may have been driven by breakoff of the India lithosphere at 25–20 Ma. Rollback of the Pamir slab and/or lithospheric convective instability drove the more prolonged retrograde metamorphism in Shakh dara until ~7 Ma (U-Pb titanite, this study) and 6–2 Ma (Ar-Ar and fission track) [Stübner *et al.*, 2013b]. In addition to the regional tectonic findings, the retention of Pb and Zr in titanite for up to 25 Myr at temperatures above ~650°C requires that usually reported closure temperature of titanite (600–700°C) be reevaluated.

Acknowledgments

This project was funded by National Science Foundation grants EAR-0838269, 0923552, and 1008760, DFG bundles TIPAGE (in particular RA 442/34, 37), and CAME (subproject TIPTIMON) from the German Federal Ministry of Education and Research (support code 03G0809). Ideas about the tectonic evolution of the Pamir matured during discussions with the TIPAGE and TIPTIMON group members, in particular Bernd Schurr and Konstanze Stübner. We thank Associate Editor Lindsay Schoenbohm, reviewer Alex Robinson, and an anonymous reviewer for their thoughtful and constructive feedback. All data for this paper, including the three previously published ages [Schmidt *et al.*, 2011], are included in the supporting information Tables S1–S3.

References

- Aleinikoff, J. N., R. P. Wintsch, C. M. Fanning, and M. J. Dorais (2002), U–Pb geochronology of zircon and polygenetic titanite from the Glastonbury Complex, Connecticut, USA: An integrated SEM, EMPA, TIMS, and SHRIMP study, *Chem. Geol.*, 188(1), 125–147.
- Aleinikoff, J. N., R. P. Wintsch, R. P. Tollo, D. M. Unruh, C. M. Fanning, and M. D. Schmitz (2007), Ages and origins of rocks of the Killingworth dome, south-central Connecticut: Implications for the tectonic evolution of southern New England, *Am. J. Sci.*, 307(1), 63–118, doi:10.2475/01.2007.04.
- Bershaw, J., C. N. Garzzone, L. Schoenbohm, G. Gehrels, and L. Tao (2012), Cenozoic evolution of the Pamir plateau based on stratigraphy, zircon, provenance, and stable isotopes of foreland basin sediments at Oytang (Wuyitake) in the Tarim Basin (west China), *J. Asian Earth Sci.*, 44, 136–148, doi:10.1016/j.jseas.2011.04.020.
- Brunel, M., N. Arnaud, P. Tapponnier, Y. Pan, and Y. Wang (1994), Kongur Shan normal fault: Type example of mountain building assisted by extension (Karakoram fault, eastern Pamir), *Geology*, 22, 707–710, doi:10.1130/0091-7613(1994)022<0707:KSNFTE>2.3.CO;2.
- Burtman, V. S., and P. Molnar (1993), Geological and geophysical evidence for deep subduction of continental crust beneath the Pamir, *Spec. Pap.-Geol. Soc. Am.*, 281, 1–76.
- Cao, K., G. C. Wang, P. van der Beek, M. Bernet, and K. X. Zhang (2013), Cenozoic thermo-tectonic evolution of the northeastern Pamir revealed by zircon and apatite fission-track thermochronology, *Tectonophysics*, 589, 17–32, doi:10.1016/j.tecto.2012.12.038.
- Cherniak, D. J. (1993), Lead diffusion in titanite and preliminary results on the effects of radiation damage on Pb transport, *Chem. Geol.*, 110(1), 177–194.
- Cherniak, D. J. (2006), Zr diffusion in titanite, *Contrib. Mineral. Petrol.*, 152(5), 639–647.
- Cherniak, D. J. (2010), Diffusion in accessory minerals: Zircon, titanite, apatite, monazite and xenotime, *Rev. Mineral. Geochem.*, 72(1), 827–869.
- Chung, S. L., D. Liu, J. Ji, M. F. Chu, H. Y. Lee, D. J. Wen, C. H. Lo, T. Y. Lee, Q. Qian, and Q. Zhang (2003), Adakites from continental collision zones: Melting of thickened lower crust beneath southern Tibet, *Geology*, 31(11), 1021–1024, doi:10.1130/G19796.1.
- Chung, S. L., M. F. Chu, Y. Zhang, Y. Xie, C. H. Lo, T. Y. Lee, C. Y. Lan, X. Li, and Y. Wang (2005), Tibetan tectonic evolution inferred from spatial and temporal variations in post-collisional magmatism, *Earth Sci. Rev.*, 68(3–4), 173–196, doi:10.1016/j.earscirev.2004.05.001.
- Compston, W., I. S. Williams, J. L. Kirschvink, Z. Zichao, and M. A. Guogan (1992), Zircon U-Pb ages for the Early Cambrian time-scale, *J. Geol. Soc.*, 149, 171–184, doi:10.1144/gsjgs.149.2.0171.
- Copley, A., J. P. Avouac, and J. Y. Royer (2010), India-Asia collision and the Cenozoic slowdown of the Indian plate: Implications for the forces driving plate motions, *J. Geophys. Res.*, 115, B03410, doi:10.1029/2009JB006634.
- Corfu, F. (1996), Multistage zircon and titanite growth and inheritance in an Archean gneiss complex, Winnipeg River Subprovince, Ontario, *Earth Planet. Sci. Lett.*, 141(1), 175–186.
- Coutand, I., M. R. Strecker, J. R. Arrowsmith, G. Hillel, R. C. Thiede, A. Korjenkov, and M. Omuraliev (2002), Late Cenozoic tectonic development of the intramontane Alai Valley, (Pamir-Tian Shan region, central Asia): An example of intracontinental deformation due to the Indo-Eurasia collision, *Tectonics*, 21, 1053, doi:10.1029/2002TC001358.
- Cowgill, E. (2010), Cenozoic right-slip faulting along the eastern margin of the Pamir salient, northwestern China, *Geol. Soc. Am. Bull.*, 122(1), 145–161, doi:10.1130/B26520.1.
- DeCelles, P. G., P. Kapp, J. Quade, and G. E. Gehrels (2011), Oligocene–Miocene Kailas basin, southwestern Tibet: Record of postcollisional upper-plate extension in the Indus-Yarlung suture zone, *Geol. Soc. Am. Bull.*, 123(7–8), 1337–1362, doi:10.1130/B30258.1.
- de Sigoyer, J., V. Chavagnac, J. Blichert-Toft, I. M. Villa, B. Luais, S. Guillot, M. Cosca, and G. Mascle (2000), Dating the Indian continental subduction and collisional thickening in the northwest Himalaya: Multichronology of the Tso Moriri eclogites, *Geology*, 28(6), 487–490, doi:10.1130/0091-7613(2000)27<487:DTICSA>2.0.CO;2.
- Ding, L., P. Kapp, and X. Wan (2005), Paleocene–Eocene record of ophiolite obduction and initial India-Asia collision, south central Tibet, *Tectonics*, 24, TC3001, doi:10.1029/2004TC001729.
- Dmitriev, E. A. (1976), *Cenozoic Potassic Alkaline Rocks in Eastern Pamir*, Donish, Dushanbe.
- Ducea, M. N., V. Lutkov, V. T. Minaev, B. Hacker, L. Ratschbacher, P. Luffi, and J. Metcalf (2003), Building the Pamirs: The view from the underside, *Geology*, 31(10), 849–852.
- Frost, B. R., K. R. Chamberlain, and J. C. Schumacher (2001), Sphene (titanite): Phase relations and role as a geochronometer, *Chem. Geol.*, 172(1), 131–148.
- Frost, C. D., and C. M. Fanning (2006), Archean geochronological framework of the Bighorn Mountains, Wyoming, *Can. J. Earth Sci.*, 43(10), 1399–1418.
- Gao, S., X. Liu, H. Yuan, B. Hattendorf, D. Günther, L. Chen, and S. Hu (2007), Determination of forty two major and trace elements in USGS and NIST SRM glasses by laser ablation-inductively coupled plasma-mass spectrometry, *J. Geostand. Geoanal.*, 26, 181–196.
- Gao, X. Y., Y. F. Zheng, Y. X. Chen, and J. Guo (2012), Geochemical and U-Pb age constraints on the occurrence of polygenetic titanites in UHP metagranite in the Dabie orogen, *Lithos*, 136–139, 93–108, doi:10.1016/j.lithos.2011.03.020.

- Gordon, S. M., P. Luffi, B. R. Hacker, J. Valley, M. Spicuzza, R. Kozdon, L. Kelemen, L. Ratschbacher, and V. Minaev (2012), The thermal structure of continental crust in active orogens: Insight from Miocene eclogite and granulite xenoliths of the Pamir mountains, *J. Metamorph. Petrol.*, 30(4), 413–434, doi:10.1111/j.1525-1314.2012.00973.x.
- Hacker, B. R., P. Luffi, V. Lutkov, V. Minaev, L. Ratschbacher, T. Plank, M. Ducea, A. Patiño-Douce, M. McWilliams, and J. Metcalf (2005), Near-ultrahigh pressure processing of continental crust: Miocene crustal xenoliths from the Pamir, *J. Petrol.*, 46(8), 1661–1687, doi:10.1093/ptology/egi030.
- Hayden, L. A., E. B. Watson, and D. A. Wark (2008), A thermobarometer for sphene (titanite), *Contrib. Mineral. Petrol.*, 155(4), 529–540.
- Ischuk, A., et al. (2013), Kinematics of the Pamir and Hindu Kush regions from GPS geodesy, *J. Geophys. Res.: Solid Earth*, 118, 2408–2416, doi:10.1002/jgrb.50185.
- Jiang, Y. H., Z. Liu, R. Y. Jia, S. Y. Liao, Q. Zhou, and P. Zhou (2012), Miocene potassic granite-syenite association in western Tibetan Plateau: Implications for shoshonitic and high Ba-Sr granite genesis, *Lithos*, 134–135, 146–162, doi:10.1016/j.lithos.2011.12.012.
- Kapp, P., P. G. DeCelles, G. E. Gehrels, M. Heizler, and L. Ding (2007), Geological records of the Lhasa-Qiantang and Indo-Asian collisions in the Nima area of central Tibet, *Geol. Soc. Am. Bull.*, 117(7–8), 917–933, doi:10.1130/B26033.1.
- Ke, S., Z. H. Luo, and X. X. Mo (2006), Mineralogy of Taxkorgan Cenozoic alkaline complex and its implications to the pluton genesis, Xianjiang, *Acta Petrol. Mineral.*, 25(2), 148–156.
- Ke, S., Z. H. Luo, X. X. Mo, W. H. Zhang, L. Tao, and H. M. Zhan (2008), The geochronology of Taxkorgan alkalic complex, Pamir syntax, *Acta Petrol. Sin.*, 24(2), 315–324.
- Kohn, M. J., and C. D. Parkinson (2002), Petrologic case for Eocene slab breakoff during the Indo-Asian collision, *Geology*, 30(7), 591–594, doi:10.1130/0091-7613(2002)030<0591:PCFESB>2.0.CO;2.
- Kylander-Clark, A. R., B. R. Hacker, and J. M. Cottle (2013), Laser-ablation split-stream ICP petrochronology, *Chem. Geol.*, 345, 99–112.
- Lee, T. Y., and L. A. Lawver (1995), Cenozoic plate reconstruction of Southeast Asia, *Tectonophysics*, 251(1–4), 85–138, doi:10.1016/0040-1951(95)00023-2.
- Li, C., R. D. van der Hilst, A. S. Meltzer, and E. R. Engahl (2008), Subduction of the Indian lithosphere beneath the Tibetan Plateau and Burma, *Earth Planet. Sci. Lett.*, 274(1–2), 157–168, doi:10.1016/j.epsl.2008.07.016.
- Lin, Q. C., B. Xia, and Y. Q. Zhang (2006), Ar-Ar dating of potassic alkali-rocks in the western Kunlun-Karakorum mountains—Example for the rocks of Yanghu, Zankan and Kuzigan, *J. Mineral. Petrol.*, 26, 66–70.
- Luo, Z. H., X. X. Mo, and S. Ke (2003), The ages of Taxkorgan alkaline intrusive complex and their implications in geological history, EGS-AGU-EUG Joint Assembly, Abstracts, #10402.
- Mahéo, G., S. Guillot, J. Blichert-Toft, Y. Rolland, and A. Pêcher (2002), A slab breakoff model for the Neogene thermal evolution of South Karakorum and South Tibet, *Earth Planet. Sci. Lett.*, 195(1–2), 45–58, doi:10.1016/S0012-821X(01)00578-7.
- Mazdab, F. K. (2009), Characterization of flux-grown trace-element-doped titanite using the high-mass-resolution ion microprobe (SHRIMP-RG), *Can. Mineral.*, 47(4), 813–831.
- Mechie, J., et al. (2012), Crustal and uppermost mantle velocity structure along a profile across the Pamir and southern Tien Shan as derived from project TIPAGE wide-angle seismic data, *Geophys. J. Int.*, 188(2), 385–407, doi:10.1111/j.1365-246X.2011.05278.x.
- Mohadjer, S., et al. (2010), Partitioning of India-Eurasia convergence in the Pamir-Hindu Kush from GPS measurements, *Geophys. Res. Lett.*, 37, L04305, doi:10.1029/2009GL041737.
- Molnar, P., and H. Lyon-Caen (1988), Some simple physical aspects of the support, structure, and evolution of mountain belts, *Spec. Pap.-Geol. Soc. Am.*, 218, 30, doi:10.1130/SPE218-p179.
- Nábělek, J., G. Hetényi, J. Vergne, S. Sapkota, B. Kafle, M. Jiang, H. Su, J. Chen, B. S. Huang, and the Hi-CLIMB (2009), Team, underplating in the Himalaya-Tibet collision zone revealed by the Hi-CLIMB experiment, *Science*, 325(5946), 1371–1374, doi:10.1126/science.1167719.
- Negredo, A. M., A. Replumaz, A. Villaseñor, and S. Guillot (2007), Modeling the evolution of continental subduction processes in the Pamir-Hindu Kush region, *Earth Planet. Sci. Lett.*, 259(1), 212–225.
- Nikolaev, V. G. (2002), Afghan-Tajik depression: Architecture of sedimentary cover and evolution, *Russ. J. Earth Sci.*, 4(6), 399–421.
- Reigber, C., G. W. Michel, R. Galas, D. Angermann, J. Klotz, J. Y. Chen, A. Papschev, R. Arslanov, V. E. Tzurkov, and M. C. Ishanov (2001), New space geodetic constraints on the distribution of deformation in Central Asia, *Earth Planet. Sci. Lett.*, 191(1–2), 157–165, doi:10.1016/S0012-821X(01)00414-9.
- Replumaz, A., A. M. Negredo, S. Guillot, and A. Villaseñor (2010), Multiple episodes of continental subduction during India/Asia convergence: Insight from seismic tomography and tectonic reconstruction, *Tectonophysics*, 483(1), 125–134.
- Rey, P., O. Vanderhaeghe, and C. Teyssier (2001), Gravitational collapse of the continental crust: Definition, regimes and modes, *Tectonophysics*, 342(3), 435–449.
- Robinson, A. C., A. Yin, C. E. Manning, T. M. Harrison, S. H. Zhang, and X. F. Wang (2004), Tectonic evolution of the northeastern Pamir: Constraints from the northern portion of the Cenozoic Kongur Shan extensional system, western China, *Geol. Soc. Am. Bull.*, 116(7–8), 953–973, doi:10.1130/B25375.1.
- Robinson, A. C., A. Yin, C. E. Manning, T. M. Harrison, S. H. Zhang, and X. F. Wang (2007), Cenozoic evolution of the eastern Pamir: Implications for strain-accommodation mechanisms at the western end of the Himalayan-Tibetan orogen, *Geol. Soc. Am. Bull.*, 119(7–8), 882–896, doi:10.1130/B25981.1.
- Rubatto, D., and J. Hermann (2001), Exhumation as fast as subduction?, *Geology*, 29(1), 3–6, doi:10.1130/0091-7613(2001)029<0003:EAFAS>2.0.C;2.
- Rutte, D., M. Stearns, and L. Ratschbacher (2013), The eastern Central Pamir Gneiss Domes: Temporal and spatial geometry of burial and exhumation, In EGU General Assembly Conference Abstracts, 15, 6090.
- Schärer, U., L. S. Zhang, and P. Tapponnier (1994), Duration of strike-slip movements in large shear zones: The Red River best China, *Earth Planet. Sci. Lett.*, 126, 379–397, doi:10.1016/0012-821X(94)90119-8.
- Schmidt, J., B. R. Hacker, L. Ratschbacher, K. Stübner, M. Stearns, A. Kylander-Clark, J. M. Cottle, A. Webb, G. Gehrels, and V. Minaev (2011), Cenozoic deep crust in the Pamir, *Earth Planet. Sci. Lett.*, 312, 411–421, doi:10.1016/j.epsl.2011.10.034.
- Schneider, F. M., et al. (2013), Seismic imaging of subducting continental lower crust beneath the Pamir, *Earth Planet. Sci. Lett.*, 375, 101–112, doi:10.1016/j.epsl.2013.05.015.
- Schurr, B., L. Ratschbacher, C. Sippl, R. Gloaguen, X. Yuan, and J. Mechie (2014), Seismotectonics of the Pamir, central Asia, *Tectonics*, 33, 1501–1518, doi:10.1002/2014TC003576.
- Schwab, G., G. Katzung, A. O. Ludwig, and H. Lützner (1980), Neogene molasse-sedimentation in der Tadschikischen depression (tadschikische SSR), *Zeitschrift für Angewandte Geologie*, 26(5), 225–238.
- Schwab, M., et al. (2004), Assembly of the Pamirs: Age and origin of magmatic belts from the southern Tien Shan to the southern Pamirs and their relation to Tibet, *Tectonics*, 23, TC4002, doi:10.1029/2003TC001583.

- Scott, D. J., and M. R. St-Onge (1995), Constraints on Pb closure temperature in titanite based on rocks from the Ungava orogen, Canada: Implications for U-Pb geochronology and PTt path determinations, *Geology*, 23(12), 1123–1126.
- Selverstone, J. (2004), Are the Alps collapsing?, *Annu. Rev. Earth Planet. Sci.*, 33, 113–132, doi:10.1146/annurev.earth.33.092203.122535.
- Sippl, C., et al. (2013a), Deep burial of Asian continental crust beneath the Pamir imaged with local earthquake tomography, *Earth Planet. Sci. Lett.*, 384, 165–177.
- Sippl, C., et al. (2013b), Geometry of the Pamir-Hindu Kush intermediate-depth earthquake zone from local seismic data, *J. Geophys. Res.: Solid Earth*, 118, 1438–1457, doi:10.1002/jgrb.50128.
- Smit, M. A., L. Ratschbacher, E. Kooijman, and M. A. Stearns (2014), Early evolution of the Pamir deep crust from Lu-Hf and U-Pb geochronology and garnet thermometry, *Geology*, doi:10.1130/G35878.1.
- Sobel, E. R., and T. A. Dumitru (1997), Thrusting and exhumation around the margins of the western Tarim basin during the India-Asia collision, *J. Geophys. Res.*, 102(B3), 5043–5063, doi:10.1029/96JB03267.
- Sobel, E. R., J. Chen, L. M. Schoenbohm, R. Thiede, D. F. Stockli, M. Sudo, and M. R. Strecker (2013), Oceanic-style subduction controls late Cenozoic deformation of the Northern Pamir orogen, *Earth Planet. Sci. Lett.*, 363, 204–218, doi:10.1016/j.epsl.2012.12.009.
- Spencer, K. J., B. R. Hacker, A. R. C. Kylander-Clark, T. B. Andersen, J. M. Cottle, M. A. Stearns, J. E. Poletti, and G. G. E. Seward (2013), Campaign-style titanite U-Pb dating by laser-ablation ICP: Implications for crustal flow, phase transformations and titanite closure, *Chem. Geol.*, 341, 84–101, doi:10.1016/j.chemgeo.2012.11.012.
- Stearns, M. A., B. R. Hacker, L. Ratschbacher, J. Lee, J. M. Cottle, and A. Kylander-Clark (2013), Synchronous Oligocene–Miocene metamorphism of the Pamir and the north Himalaya driven by plate-scale dynamics, *Geology*, 41(10), 1071–1074.
- Stübner, K., L. Ratschbacher, D. Rutte, K. Stanek, V. Minaev, M. Wiesinger, and R. Gloaguen (2013a), The giant Shakh-dara migmatitic gneiss dome, Pamir, India-Asia collision zone: 1, *Tectonics*, 32(4), 948–979, doi:10.1002/tect.20059.
- Stübner, K., et al. (2013b), The giant Shakh-dara migmatitic gneiss dome, Pamir, India-Asia collision zone: 2 Timing of dome formation, *Tectonics*, 32(5), 1404–1431, doi:10.1002/tect.20059.
- Thiede, R. C., E. R. Sobel, J. Chen, L. M. Schoenbohm, D. F. Stockli, M. Sudo, and M. R. Strecker (2013), Late Cenozoic extension and crustal doming in the India-Eurasia collision zone: New thermochronologic constraints from the NE Chinese Pamir, *Tectonics*, 32, 763–779, doi:10.1002/tect.20050.
- van Hinsbergen, D. J. J., P. Kapp, G. Dupont-Nivet, P. C. Lippert, P. G. DeCelles, and T. H. Torsvik (2011), Restoration of Cenozoic deformation in Asia and the size of Greater India, *Tectonics*, 30, TC5003, doi:10.1029/2011TC002908.
- Vermeesch, P. (2012), On the visualisation of detrital age distributions, *Chem. Geol.*, 312, 190–194.
- Vlasov, N. G., Y. A. Dyakov, and E. S. Cherev (1991), *Geological Map of the Tajik SSR and Adjacent Territories, 1:500,000*, VSEGEI, Leningrad.
- Wendt, I., and C. Carl (1991), The statistical distribution of the mean squared weighted deviation, *Chem. Geol.: Isot. Geosci. Sect.*, 86(4), 275–285, doi:10.1016/0168-9622(91)90010-T.
- Xu, R. H., Y. Q. Zhang, X. Xie, P. Vidal, N. Arnaud, Q. Zhang, and D. Zhao (1996), Isotopic geochemistry of plutonic rock, in *Geological Evolution of the Karakorum and Kunlun Mountains* [in Chinese], edited by Y. S. Pan, pp. 137–186, Seismological Press, Beijing.
- Zhang, L. S., and U. Schärer (1996), Inherited Pb components in magmatic titanite and their consequence for the interpretation of U-Pb ages, *Earth Planet. Sci. Lett.*, 138, 57–65, doi:10.1016/0012-821X(95)00237-7.
- Zubovich, A. V., et al. (2010), GPS velocity field for the Tien Shan and surrounding regions, *Tectonics*, 29, TC6014, doi:10.1029/2010TC002772.